ORNL/TM-2024/3265

Threat Sources for Creating Synthetic Urban Search Data

Douglas E. Peplow
Daniel E. Archer
Andrew D. Nicholson
Nicholas J. Prins
Mark S. Bandstra
et al.

February 2024

OAK RIDGE National Laboratory

ORNL IS MANAGED BY UT-BATTELLE LLC FOR THE US DEPARTMENT OF ENERGY

ORNL/TM-2024/3265

Nuclear Energy and Fuel Cycle Division

THREAT SOURCES FOR CREATING SYNTHETIC URBAN SEARCH DATA

Douglas E. Peplow*
Daniel E. Archer*
Andrew D. Nicholson*
Nicholas J. Prins*
Mark S. Bandstra†
A. Chandler Jones†
Brian J. Quiter†
Abigael C. Nachtsheim‡
James M. Ghawaly Jr.§

*Oak Ridge National Laboratory
†Lawrence Berkeley National Laboratory
‡Los Alamos National Laboratory
§Louisiana State University Security Programs Institute

February 2024

Prepared by
OAK RIDGE NATIONAL LABORATORY
Oak Ridge, TN 37831-6283
managed by
UT-BATTELLE LLC
for the
US DEPARTMENT OF ENERGY
under contract DE-AC05-00OR22725

CONTENTS

LIST OF FIGURES iv
LIST OF TABLES vi
ABBREVIATIONS vii
ABSTRACT viii
1. INTRODUCTION 1
2. BASIC ISOTOPIC SOURCES 2
2.1 SOURCES LISTED IN THE N42 STANDARDS 2
2.2 DEVELOPING SOURCES FOR RADAI/REX 2
2.3 CALCULATED EMISSION SPECTRA 3
2.4 EQUIVALENT POINT SOURCE EMISSION SPECTRA 6
2.5 ESTIMATED SODIUM IODIDE DETECTOR RESPONSES 9
2.6 BASIC SOURCES WITH POLYMETHYL METHACRYLATE 11
3. MEDICAL SOURCES 16
3.1 SOURCES LISTED IN THE N42 STANDARDS 16
3.2 DEVELOPING SOURCES FOR RADAI/REX 16
3.3 ADDITIONAL MEDICAL SOURCES 17
3.4 CALCULATED EMISSION SPECTRA 17
3.5 EQUIVALENT POINT SOURCE EMISSION SPECTRA 19
3.6 ESTIMATED SODIUM IODIDE DETECTOR RESPONSES 21
4. INDUSTRIAL SOURCES 23
4.1 DEVELOPING SOURCES FOR RADAI/REX 23
4.2 CALCULATED EMISSION SPECTRA 24
4.3 EQUIVALENT POINT SOURCE EMISSION SPECTRA 24
4.4 ESTIMATED SODIUM IODIDE DETECTOR RESPONSES 27
5. SPECIAL NUCLEAR MATERIAL 29
5.1 SOURCES LISTED IN THE N42 STANDARDS 29
5.2 DEVELOPING SOURCES FOR RADAI/REX 30
5.3 CALCULATED EMISSION STRENGTH AND SPECTRA 30
5.4 EQUIVALENT POINT SOURCE EMISSION SPECTRA 33
5.5 ESTIMATED SODIUM IODIDE DETECTOR RESPONSES 39
6. SUMMARY 42
7. REFERENCES 44

LIST OF FIGURES

Figure 1. Emission spectrum for ^{40}K. 3
Figure 2. Emission spectrum for ^{57}Co. 4
Figure 3. Emission spectrum for ^{60}Co. 4
Figure 4. Emission spectrum for ^{137}Cs. 4
Figure 5. Emission spectrum for ^{133}Ba. 5
Figure 6. Emission spectrum for ^{192}Ir. 5
Figure 7. Emission spectrum for ^{226}Ra. 5
Figure 8. Emission spectrum for ^{232}Th. 6
Figure 9. Emission spectrum for ^{241}Am. 6
Figure 10. Equivalent point source emission spectra for (left) ^{40}K and (right) ^{57}Co. 8
Figure 11. Equivalent point source emission spectra for (left) ^{60}Co and (right) ^{137}Cs. 8
Figure 12. Equivalent point source emission spectra for (left) ^{133}Ba and (right) ^{192}Ir. 8
Figure 13. Equivalent point source emission spectra for (left) ^{226}Ra and (right) ^{232}Th. 9
Figure 14. Equivalent point source emission spectrum for ^{241}Am. 9
Figure 15. Predicted NaI count rate spectra for (left) ^{40}K and (right) ^{57}Co. 9
Figure 16. Predicted NaI count rate spectra for (left) ^{60}Co and (right) ^{137}Cs. 10
Figure 17. Predicted NaI count rate spectra for (left) ^{133}Ba and (right) ^{192}Ir. 10
Figure 18. Predicted NaI count rate spectra for (left) ^{226}Ra and (right) ^{232}Th. 10
Figure 19. Predicted NaI count rate spectrum for ^{241}Am. 11
Figure 20. Equivalent point source emission spectra for (left) ^{40}K and (right) ^{57}Co shielded with PMMA. 11
Figure 21. Equivalent point source emission spectra for (left) ^{60}Co and (right) ^{137}Cs shielded with PMMA. 12
Figure 22. Equivalent point source emission spectra for (left) ^{133}Ba and (right) ^{192}Ir shielded with PMMA. 12
Figure 23. Equivalent point source emission spectra for (left) ^{226}Ra and (right) ^{232}Th shielded with PMMA. 12
Figure 24. Equivalent point source emission spectra for ^{241}Am shielded with PMMA. 13
Figure 25. Predicted NaI count rate spectra for (left) ^{40}K and (right) ^{57}Co shielded with PMMA. 13
Figure 26. Predicted NaI count rate spectra for (left) ^{60}Co and (right) ^{137}Cs shielded with PMMA. 13
Figure 27. Predicted NaI count rate spectra for (left) ^{133}Ba and (right) ^{192}Ir shielded with PMMA. 14
Figure 28. Predicted NaI count rate spectra for (left) ^{226}Ra and (right) ^{232}Th shielded with PMMA. 14
Figure 29. Predicted NaI count rate spectra for ^{241}Am shielded with PMMA. 14
Figure 30. Emission spectrum for ^{67}Ga. 18
Figure 31. Emission spectrum for ^{99m}Tc. 18
Figure 32. Emission spectrum for ^{131}I. 18
Figure 33. Emission spectrum for ^{133}Xe. 19
Figure 34. Emission spectrum for ^{177}Lu. 19
Figure 35. Emission spectrum for ^{201}Tl. 19
Figure 36. Equivalent point source emission spectra for (left) ^{67}Ga and (right) ^{99m}Tc. 20
Figure 37. Equivalent point source emission spectra for (left) ^{131}I and (right) ^{133}Xe. 20
Figure 38. Equivalent point source emission spectra for (left) ^{177}Lu and (right) ^{201}Tl. 21
Figure 39. Predicted NaI count rate spectra for (left) ^{67}Ga and (right) ^{99m}Tc. 21
Figure 40. Predicted NaI count rate spectra for (left) ^{131}I and (right) ^{133}Xe. 22
Figure 41. Predicted NaI count rate spectra for (left) ^{177}Lu and (right) ^{201}Tl. 22
Figure 42. (left) Equivalent point source emission spectra and (right) predicted NaI count rate spectra for a pure 511 keV emmitter. 22
Figure 43. ^{90}Sr/^{90}Y beta spectra from ORIGEN. 23

Figure 44. ^{67}Cu photon emission spectrum. 24
Figure 45. ^{192}Ir photon emission spectra. 24
Figure 46. DU photon emission spectra. 24
Figure 47. Equivalent point source emission spectra for (left) ^{67}Cu and (right) ^{90}Sr/^{90}Y. 25
Figure 48. Equivalent point source emission spectrum for ^{192}Ir in steel. 25
Figure 49. Equivalent point source emission spectra for ^{192}Ir inside shells of DU and (right) shells of DU. 26
Figure 50. Predicted NaI count rate spectra for (left) ^{67}Cu and (right) ^{90}Sr/^{90}Y. 27
Figure 51. Predicted NaI count rate spectrum for ^{192}Ir in steel. 28
Figure 52. Predicted NaI count rate spectra for ^{192}Ir in (left) DU shells and (right) DU shells. 28
Figure 53. Predicted NaI count rate spectra for different activities of ^{192}Ir in a 15 mm shell of DU. 28
Figure 54. Emission spectrum for DU. 31
Figure 55. Emission spectrum for U ore. 31
Figure 56. Emission spectrum for refined U. 31
Figure 57. Emission spectrum for LEU. 32
Figure 58. Emission spectrum for HEU. 32
Figure 59. Emission spectrum for ^{238}Pu. 32
Figure 60. Emission spectrum for PGPu. 33
Figure 61. Emission spectrum for FGPu. 33
Figure 62. Emission spectrum for WGPu. 33
Figure 63. Equivalent point source emission spectra for DU. 35
Figure 64. Equivalent point source emission spectra for U ore. 35
Figure 65. Equivalent point source emission spectra for refined U. 36
Figure 66. Equivalent point source emission spectra for LEU. 36
Figure 67. Equivalent point source emission spectra for HEU. 36
Figure 68. Equivalent point source emission spectra for ^{238}Pu. 37
Figure 69. Equivalent point source emission spectra for PGPu. 37
Figure 70. Equivalent point source emission spectra for FGPu. 37
Figure 71. Equivalent point source emission spectra for WGPu. 38
Figure 72. Predicted NaI count rate spectra for DU. 39
Figure 73. Predicted NaI count rate spectra for U ore. 39
Figure 74. Predicted NaI count rate spectra for refined U. 39
Figure 75. Predicted NaI count rate spectra for LEU. 40
Figure 76. Predicted NaI count rate spectra for HEU. 40
Figure 77. Predicted NaI count rate spectra for ^{238}Pu. 40
Figure 78. Predicted NaI count rate spectra for PGPu. 41
Figure 79. Predicted NaI count rate spectra for FGPu. 41
Figure 80. Predicted NaI count rate spectra for WGPu. 41

LIST OF TABLES

Table 1. N42 standards describing test sources 1
Table 2. Basic isotopic sources listed in the N42 standards 2
Table 3. Simulating the emission spectra for basic isotopic sources 3
Table 4. Emission strengths and equivalent point source strengths of the basic isotopes 15
Table 5. Medical sources listed in the N42 standards 16
Table 6. Contaminants in medical sources 16
Table 7. Emission strengths and equivalent point source strengths of the medical isotope sources 21
Table 8. Emission strengths and equivalent point source strengths of the industrial sources 27
Table 9. SNM sources list in the N42 standards 29
Table 10. Enghauser's typical U mass percentages 29
Table 11. Plutonium compositions from DOE Standard 3013-2018 30
Table 12. Emission strengths and equivalent point source strengths of the U and Pu sources 38
Table 13. Equivalent point source emission spectra files for MCNP, SCALE/MAVRIC, and Shift 43

ABBREVIATIONS

DOE	US Department of Energy
DRAG	Detection Radiation Algorithms Group
DU	depleted U
FGPu	fuel-grade Pu
HEU	highly enriched U
IAEA	International Atomic Energy Agency
LEU	low-enriched U
MC	Monte Carlo
MCNP	Monte Carlo N-Particle
N42	National Committee on Radiation Instrumentation
PGPu	power-grade Pu
PMMA	polymethyl methacrylate
RADAI	Radiological Anomaly Detection and Identification
REX	RADAI-Extended
RGPu	reactor-grade Pu
SNM	special nuclear material
WGPu	weapons-grade Pu

ABSTRACT

Equivalent point source energy emission distributions were computed for various threat sources for use in simulating the detector responses for urban search scenarios. The sources include standard isotopic sources used in detector testing, medical and industrial sources occasionally encountered in urban searches, and several types of special nuclear materials. Most of the equivalent point source distributions represent small sources inside some amount of shielding, but the special nuclear material sources represent volumetrically distributed sources in spheres of metal. Text-based inputs for emission distributions are available for the Monte Carlo transport codes Monte Carlo N-Particle, SCALE/MAVRIC, and Omnibus/Shift, any of which can easily be converted to other formats. These sources were developed for use in the Radiological Anomaly Detection and Identification (RADAI) project and the follow-on project, the RADAI-Extended project, sponsored by the National Nuclear Security Administration Office of Defense Nuclear Nonproliferation Research and Development.

1. INTRODUCTION

The goals of the Radiological Anomaly Detection and Identification (RADAI) project and its extension, the RADAI-Extended (REX) project, are to develop large Monte Carlo (MC)–based synthetic datasets for urban search and to use those datasets to develop and compare anomaly detection and identification algorithms. The RADAI project was—and the REX project is—sponsored by the National Nuclear Security Administration Office of Defense Nuclear Nonproliferation Research and Development. The projects have been led by Lawrence Berkeley National Laboratory and have included researchers from Oak Ridge National Laboratory, Los Alamos National Laboratory, and the Louisiana State University Security Programs Institute. The RADAI/REX dataset needs to be very large and include the characteristics of real urban searches: a background with components that vary in both proportion and magnitude, a large variety of possible threat sources, and changes in background caused by rain and street clutter. The MC models used to generate the synthetic dataset were based on the work done for the National Nuclear Security Administration–sponsored urban search data competitions [1] [2] [3]. A wider variety of urban geometries will be used, as well as a more extensive set of possible threat sources. This report focuses on developing a set of sources, specifically the equivalent point source emission spectra that includes the effects of shielding, that can be used in the RADAI/REX projects and in other projects that seek to model different scenarios with a wide range of potential threat sources.

Several standards [4] [5] [6] [7] [8] from the National Committee on Radiation Instrumentation (N42) were reviewed to develop a list of sources commonly used in the testing of radiation detectors. These sources should be a good representation of the sources that are important for the search community to detect and identify, which would make them appropriate for RADAI/REX and other detection modeling projects. The American National Standards Institute standards list a variety of testing sources. In this report, the sources are organized into four categories: (1) basic isotopic sources, (2) medical sources, (3) industrial sources, and (4) materials related to special nuclear material (SNM) sources. The standards used are listed in Table 1. Other sources of information used in developing the source emission spectra are also used in the following sections to develop sources.

Table 1. N42 standards describing test sources

Standard	Title
N42.34	Performance Criteria for Handheld Instruments for the Detection and Identification of Radionuclides
N42.35	Evaluation and Performance of Radiation Detection Portal Monitors for Use in Homeland Security
N42.38	Performance Criteria for Spectroscopy-Based Portal Monitors Used in Homeland Security
N42.43	Performance Criteria for Mobile and Transportable Radiation Monitors Used for Homeland Security
N42.53	Performance Criteria for Backpack-Based Radiation-Detection Systems Used for Homeland Security

2. BASIC ISOTOPIC SOURCES

2.1 SOURCES LISTED IN THE N42 STANDARDS

Table 2 lists the basic isotopic sources used in detector testing that are described in the various N42 standards. The standards note that the "gamma-ray source activities are based on encapsulation in 0.25 mm wall thickness stainless steel" and that "^{232}Th and ^{226}Ra are in equilibrium with its progeny" [5]. Note that activity is defined not as the number of gamma rays emitted but is instead the number of decays per unit of time, which does not depend on encapsulation.

Table 2. Basic isotopic sources listed in the N42 standards

Isotope	Half-life	Strength	Comments
^{40}K	1.27×10^9 years	—	—
^{57}Co	271.8 days	5 or 10 μCi	—
^{60}Co	5.271 years	7 μCi	—
^{137}Cs	30.07 years	16 μCi	—
^{133}Ba	10.53 years	10 or 14 μCi	—
^{192}Ir	78.83 days	—	—
^{226}Ra	1,599 years	8 μCi	daughters ^{214}Bi, ^{214}Pb
^{232}Th	1.4×10^{10} years	14 μCi	daughters ^{228}Th, ^{232}U
^{241}Am	432.7 years	47 μCi	no Pu

2.2 DEVELOPING SOURCES FOR RADAI/REX

The SCALE/ORIGEN code [9] can be used to find the x-ray and gamma-ray emission spectra from radionuclides. Seven of the basic isotope sources emit beta particles, and ORIGEN can include an estimate of the bremsstrahlung spectra in the total emission spectra. ORIGEN was designed for reactor calculations, so it only has three choices of material for bremsstrahlung generation: none, in water, or in UO_2. For the RADAI/REX application, water was chosen for the bremsstrahlung generation. ORIGEN simulations do not have any geometry—the bremsstrahlung distribution from beta particles slowing down in the selected medium is added the photon line distribution. Table 3 lists the daughter products and the details about the parameters in the ORIGEN simulations.

The isotopes ^{40}K, ^{57}Co, ^{60}Co, ^{133}Ba, and ^{192}Ir decay to stable elements, so their radiation spectra do not change over time. The daughter products of the ^{137}Cs, ^{226}Ra, and ^{232}Th isotopes have very short half-lives compared with those of their parent isotopes. To allow the buildup of the daughters to secular equilibrium, aging these isotopes by one half-life of the parent will suffice. For ^{241}Am, the half-life of ^{237}Np is much longer, so it will build up nearly linearly for the first few hundred years. However, the activities of ^{237}Np and ^{233}Pa are so small (each 13.5 μBq/Bq of ^{241}Am at 43.26 years, or 0.1 of an ^{241}Am half-life) that the emission spectra do not appreciably change over short times.

Table 3. Simulating the emission spectra for basic isotopic sources

Isotope	Daughter products	Betas	Aged
^{40}K	—	Yes	—
^{57}Co	—	No	—
^{60}Co	—	Yes	—
^{137}Cs	^{137m}Ba	Yes	1 ^{137}Cs half-life
^{133}Ba	—	No	—
^{192}Ir	—	Yes	—
^{226}Ra	^{206}Tl, ^{210}Tl, ^{210}Pb, ^{214}Pb, ^{210}Bi, ^{214}Bi, ^{210}Po, ^{214}Po, ^{218}Po, ^{218}At, ^{218}Rn, ^{222}Rn	Yes	1 ^{226}Ra half-life
^{232}Th	^{208}Tl, ^{212}Pb, ^{212}Bi, ^{212}Po, ^{216}Po,^{220}Rn, ^{224}Ra, ^{228}Ra, ^{228}Ac, ^{228}Th	Yes	1 ^{232}Th half-life
^{241}Am	^{233}Pa, ^{237}Np	Yes	0.1 ^{241}Am half-life

2.3 CALCULATED EMISSION SPECTRA

The ORIGEN spectra from the basic isotopic sources are shown in Figures 1–9. Each figure contains two plots: the left plot shows the emission spectrum with linear vertical axis, and the right plot shows the spectrum using a logarithmic vertical axis. Both plots are shown so the reader can see which lines are emitted most (linear) and also see the details of the less likely emissions. Note that these emission distributions contain lines for the x-rays/gamma rays emitted and could have a continous bremsstrahlung component from the beta rays slowing down. No geometry or scatter is shown in these distributions.

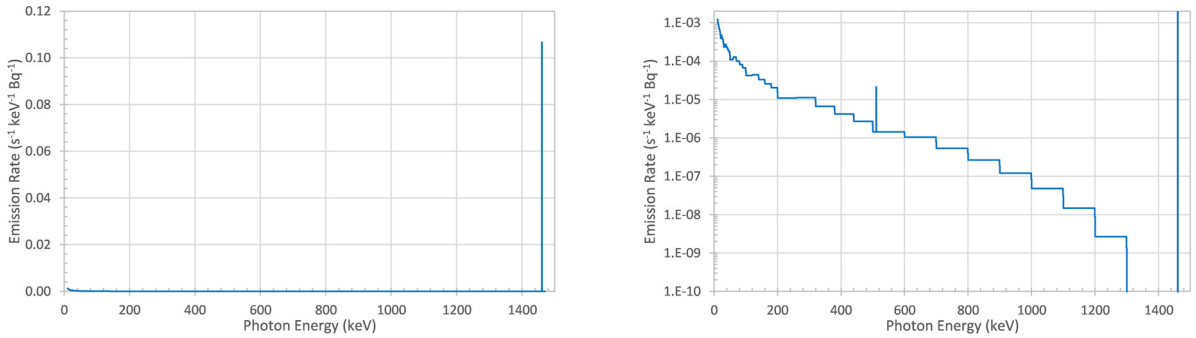

Figure 1. Emission spectrum for ^{40}K. (left) Linear vertical axis and (right) logarithmic vertical axis.

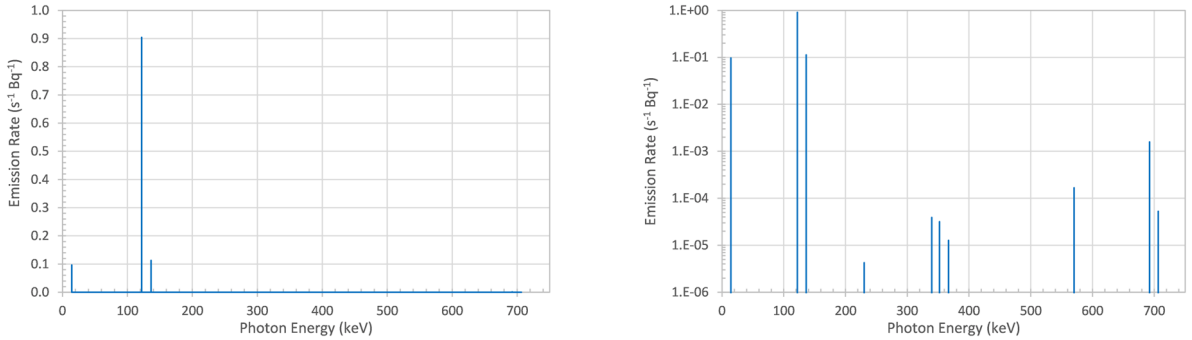

Figure 2. Emission spectrum for ^{57}Co. (left) Linear vertical axis and (right) logarithmic vertical axis.

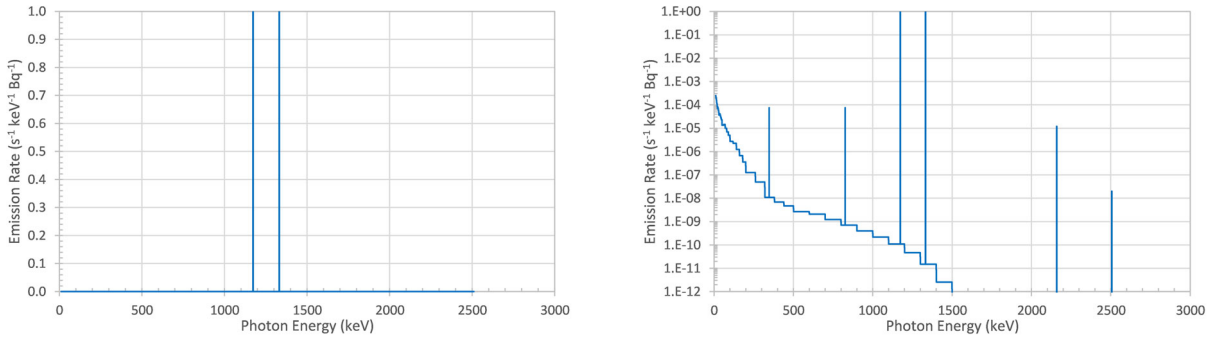

Figure 3. Emission spectrum for ^{60}Co. (left) Linear vertical axis and (right) logarithmic vertical axis.

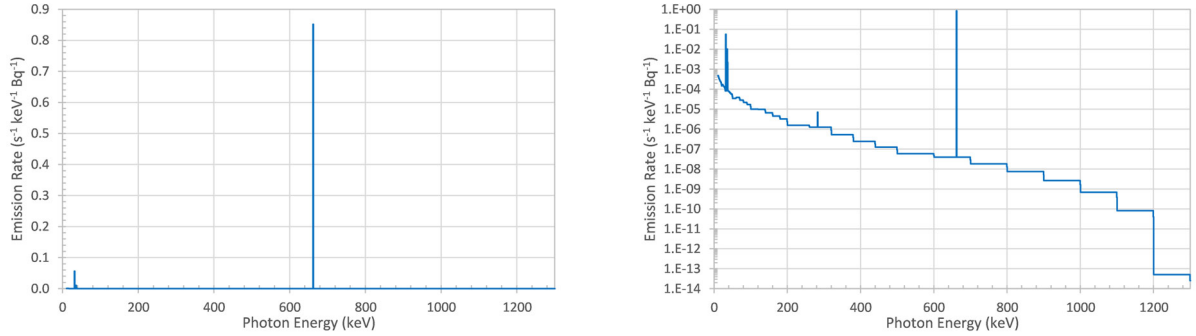

Figure 4. Emission spectrum for ^{137}Cs. (left) Linear vertical axis and (right) logarithmic vertical axis.

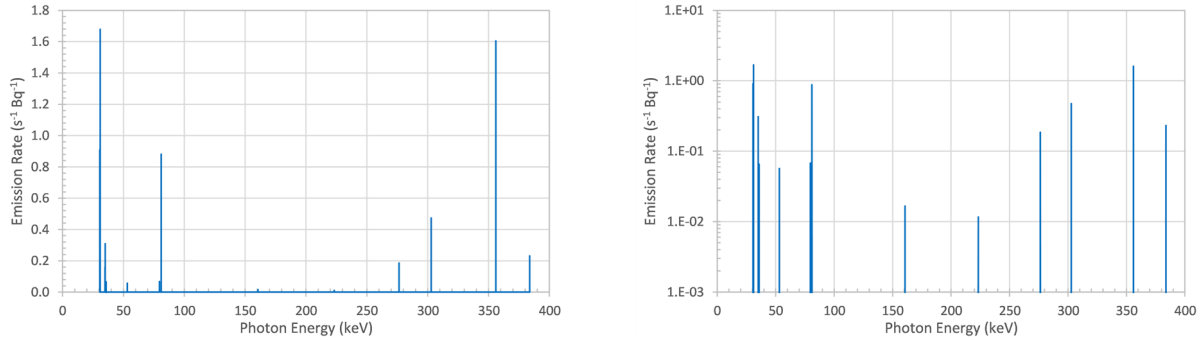

Figure 5. Emission spectrum for ^{133}Ba. (left) Linear vertical axis and (right) logarithmic vertical axis.

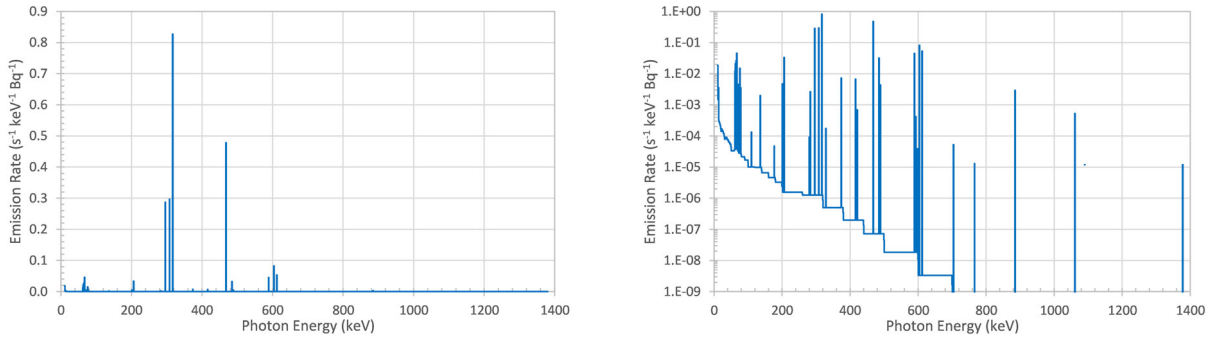

Figure 6. Emission spectrum for ^{192}Ir. (left) Linear vertical axis and (right) logarithmic vertical axis.

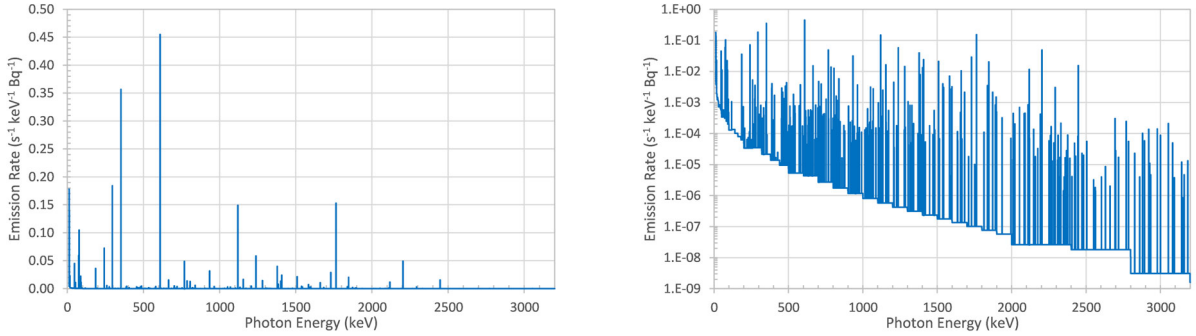

Figure 7. Emission spectrum for ^{226}Ra. (left) Linear vertical axis and (right) logarithmic vertical axis.

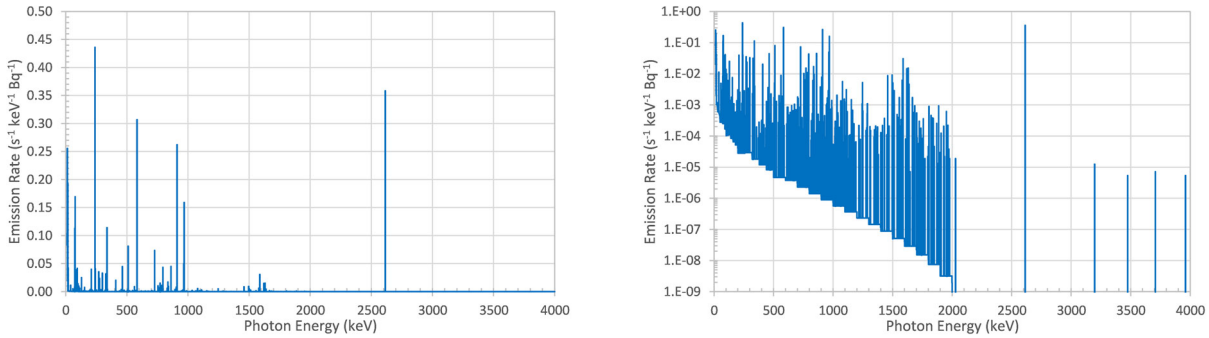

Figure 8. Emission spectrum for ^{232}Th. (left) Linear vertical axis and (right) logarithmic vertical axis.

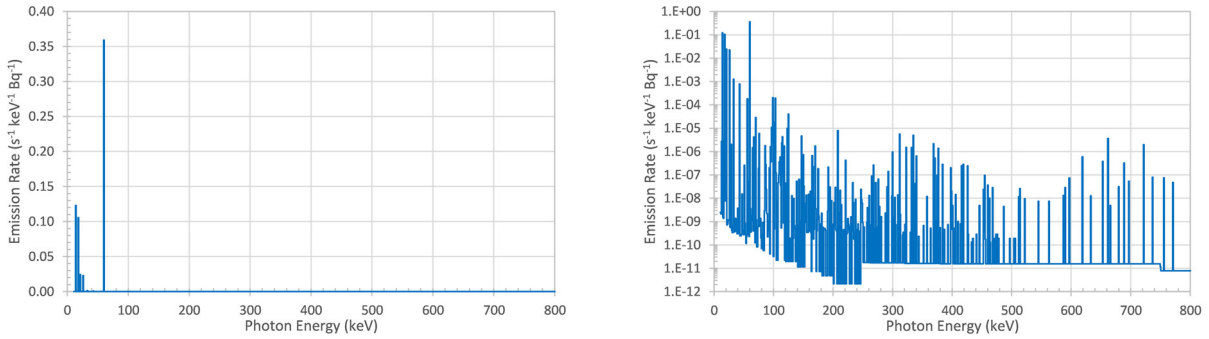

Figure 9. Emission spectrum for ^{241}Am. (left) Linear vertical axis and (right) logarithmic vertical axis.

2.4 EQUIVALENT POINT SOURCE EMISSION SPECTRA

The ORIGEN emission rates were used in SCALE/MAVRIC calculations to compute the energy-dependent flux escaping through a shield and tallied at a large distance away—the equivalent point source emission spectrum—for each source. Two shields were simulated: one with a thin 0.25 mm encapsulation layer of steel (essentially bare) and one with a 1 cm layer of steel. The point source was simulated inside a 1 cm radius void volume, surrounded by the steel shell. The equivalent point source spectra are shown in Figures 10–14.

The equivalent point source emission spectra were computed using MC, so some statistical uncertainty exists in the results. Typically, the uncertainties are inversely proportional to the square root of the emission intensity. Uncertainties are smaller for portions of the spectra that have higher values. This section contains a discussion of each source and what level of uncertainties the source distribution contains as a function of energy. The quoted energy regions are usually between prominent peaks, with the peaks themselves having smaller relative uncertainties than the regions between peaks—typically very small uncertainties (0.001% to 0.01%). In many of the spectra plots, the areas of higher relative uncertainty are noticeable as areas of low values that should be relatively smooth between peaks but instead show random fluctuations. Below 50 keV, typical uncertainties are very large because not many photons survive through the shielding layers.

For ^{40}K in 0.25 mm of steel, the relative uncertainty at 100 keV is 0.1% and rises to 1% at 1,000 keV. Uncertainties between 1,000 keV and the full-energy peak of 1,461 keV are 1%. The full-energy peak itself has an uncertainty of 0.001%. For ^{40}K in 1 cm of steel, the relative uncertainties are lower, increasing from 0.1% at 150 keV up to 0.2% near the full-energy peak and then 0.002% at the full-energy

peak. The 1 cm shell scatters many more of the full-energy photons, increasing the numbers of lower-energy photons and reducing their statistical uncertainty.

Uncertainties for ^{57}Co with 0.25 mm of steel are very small below the prominent peaks, 10%–20% between 140 keV and 190 keV, and 5%–9% between 200 keV and 700 keV. Uncertainties for the 1 cm steel casing are approximately 2% for most of the energy range and very small below the prominent peaks.

For ^{60}Co, uncertainties with 0.25 mm of steel are 2% from 100–200 keV, 1% up to 1,173 keV, and 1.3% up to 1,332 keV. The two peaks have uncertainties of less than 0.01%. Above 1,332 keV, the results are not well converged because of the small probabilities of the higher-energy emissions. With 1 cm of steel, uncertainties are less than 0.3% from 100 keV through the full-energy peaks. Similar to the bare source, results are not well converged above the 1,332 keV peak.

The uncertainties for ^{137}Cs with 0.25 mm of steel are all less than 0.8% between 100 and 190 keV, approximately 0.4% up to 662 keV, and then less than 0.01% at 662 keV. With 1 cm of steel, uncertainties are 0.1% from 150 to 662 keV and less than 0.01% at 662 keV. Uncertainties increase quickly for energies above the 662 keV peak.

The ^{133}Ba distributions have uncertainties below 1% between 100 and 383 keV, with the range of 150–356 keV having uncertainties of 0.3% for the 0.25 mm steel and 0.1% for the 1 cm steel cases.

Uncertainties for ^{192}Ir generally increase with increasing energy because of the lower probabilities of emission at higher energies. For the bare case, uncertainties are less than 0.7% from 100 to 467 keV, 1.5% up to 589 keV, 15% up to 884 keV, and then very large. With 1 cm of steel, uncertainties are 0.1% from 100 to 317 keV, 0.15% up to 467 keV, 0.3% up to 589 keV, 3% up to 884 keV, and then not well converged above 884 keV.

The ^{226}Ra uncertainties increase as the distribution probability falls. With only 0.25 mm of steel, uncertainties increase from 0.3% at 100 keV to 1% at 500 keV, 2% at 1,000 keV, 4% at 1,500 keV, and 5% at 1,764 keV. From 1,764 to 2,205 keV, the uncertainties increase to 11% then to 25% at 2,504 keV. Above 2,504 keV, uncertainties are large. For 1 cm of steel, uncertainties are less than 1% from 100 to 1,764 keV, up to 2% at 2,205 keV, up to 5% up to 2,447 keV, and then up to 20% at 2,800 keV.

Uncertainties for ^{232}Th in the bare case increase from 0.5% at 100 keV to 1% at 500 keV, 2% at 900 keV, 4% at 1,000 keV, 7% at 1,700 keV, and 7% at 2,600 keV. Above 2,600 keV, the results are not well converged. With 1 cm of steel, uncertainties are 0.2% at 100 keV, 0.3% at 500 keV, 0.8% at 1,000 keV, 1% at 1,600 keV, and then 1.2% from 1,700 to 2,600 keV. Above 2,600 keV, uncertainties are very high.

The ^{241}Am uncertainties above 120 keV at 20% increase with energy for the bare case. For the case of 1 cm of steel, uncertainties are 5% at 120 keV, increase to 20% at 400 keV, and then increase above 20% at 660 keV to very large levels.

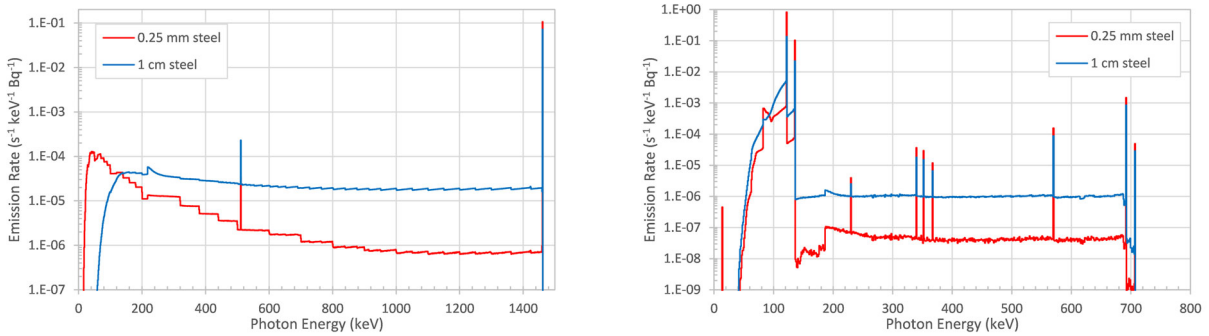

Figure 10. Equivalent point source emission spectra for (left) ^{40}K and (right) ^{57}Co. Red lines represent bare sources (with 0.25 mm steel), and blue lines represent sources shielded with 1 cm steel.

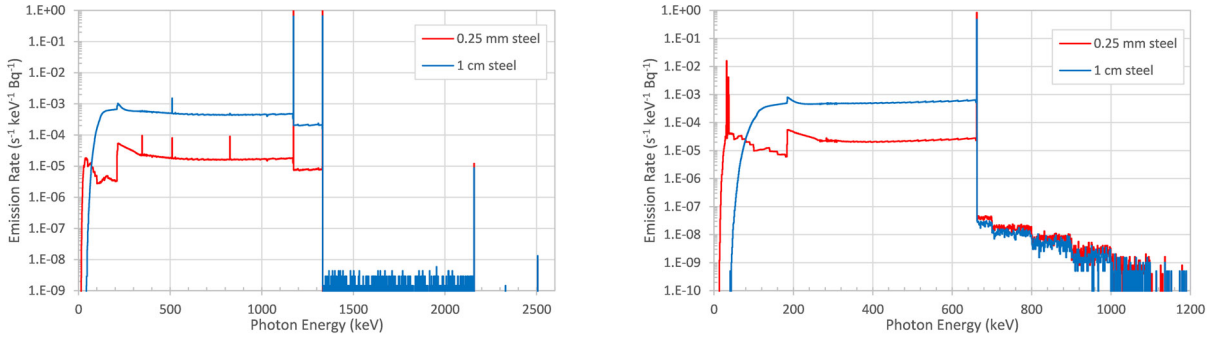

Figure 11. Equivalent point source emission spectra for (left) ^{60}Co and (right) ^{137}Cs. Red lines represent bare sources (with 0.25 mm steel), and blue lines represent sources shielded with 1 cm steel.

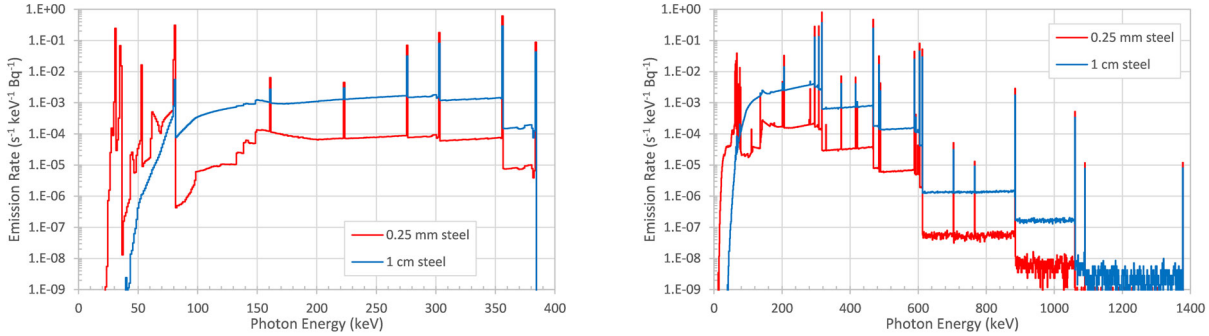

Figure 12. Equivalent point source emission spectra for (left) ^{133}Ba and (right) ^{192}Ir. Red lines represent bare sources (with 0.25 mm steel), and blue lines represent sources shielded with 1 cm steel.

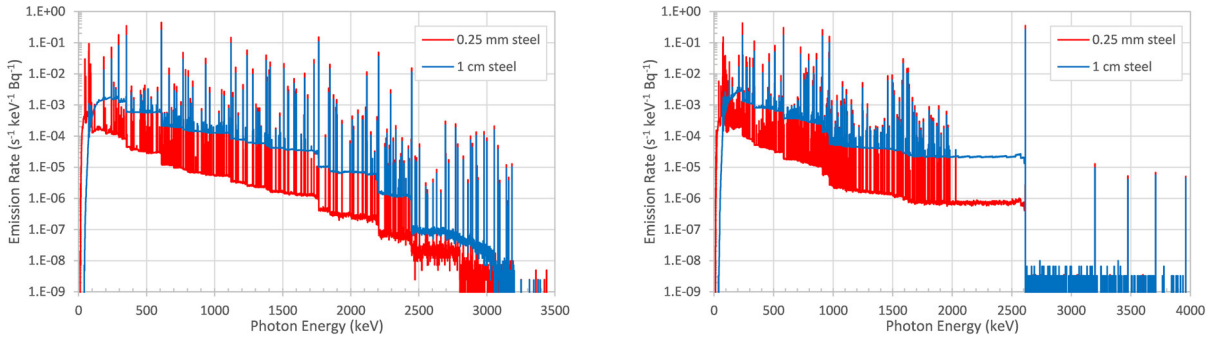

Figure 13. Equivalent point source emission spectra for (left) ^{226}Ra and (right) ^{232}Th. Red lines represent bare sources (with 0.25 mm steel), and blue lines represent sources shielded with 1 cm steel.

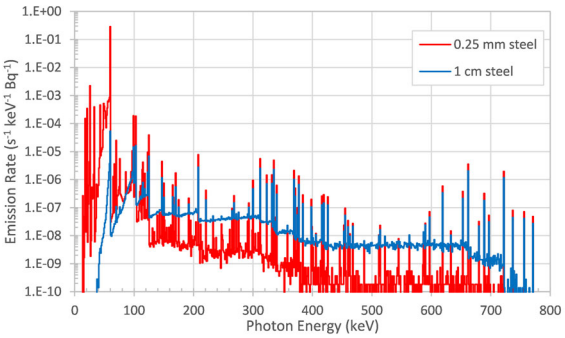

Figure 14. Equivalent point source emission spectrum for ^{241}Am. The red line represents the bare source (with 0.25 mm steel), and the blue line represents the source shielded with 1 cm steel.

2.5 ESTIMATED SODIUM IODIDE DETECTOR RESPONSES

The equivalent point source emission spectra were combined with a simple response function for photons striking the largest face of a 2 × 4 × 16 in. NaI detector. Figures 15–19 show the count rates for a detector located at a distance R from the source, multiplied by $4\pi R^2$. Units of the y-axis are counts per second-kiloelectron volt-becquerel. To compute the predicted count rate at a distance of R, the values in the plots should be multiplied by the source strength in becquerels, divided by $4\pi R^2$, and then multiplied by the area of the detector face (412.9024 cm^2).

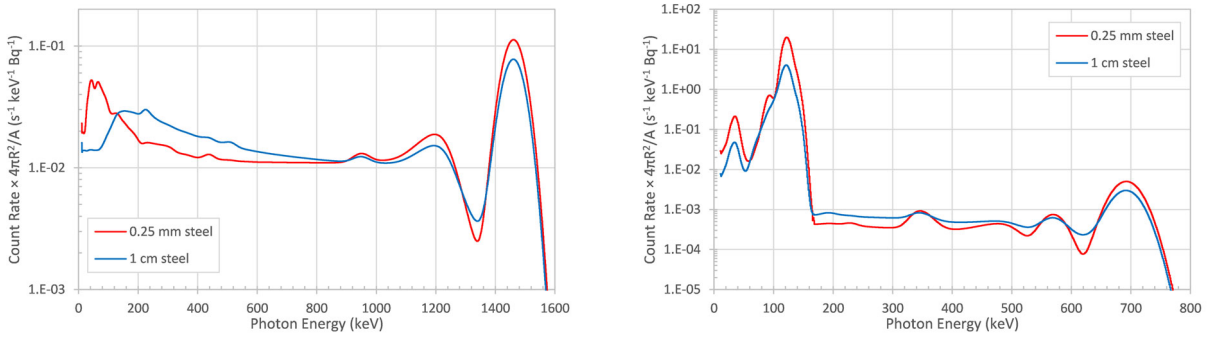

Figure 15. Predicted NaI count rate spectra for (left) ^{40}K and (right) ^{57}Co. Red lines represent bare sources (with 0.25 mm steel), and blue lines represent sources shielded with 1 cm steel.

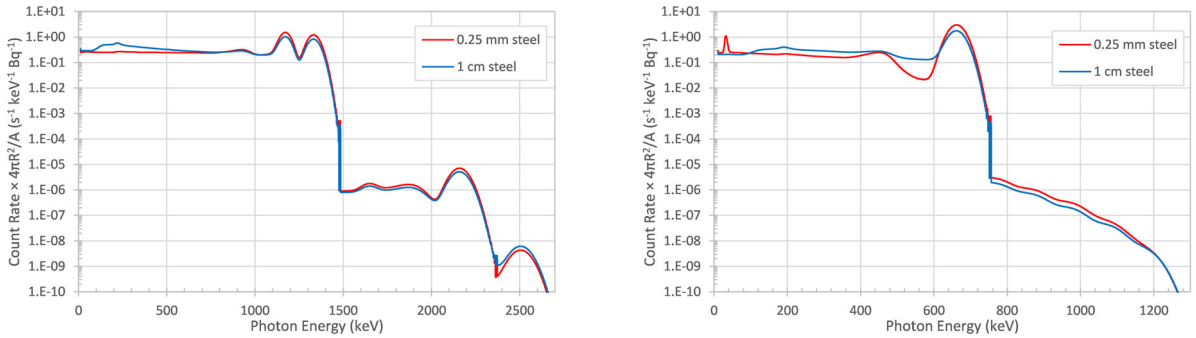

Figure 16. Predicted NaI count rate spectra for (left) ^{60}Co and (right) ^{137}Cs. Red lines represent bare sources (with 0.25 mm steel), and blue lines represent sources shielded with 1 cm steel.

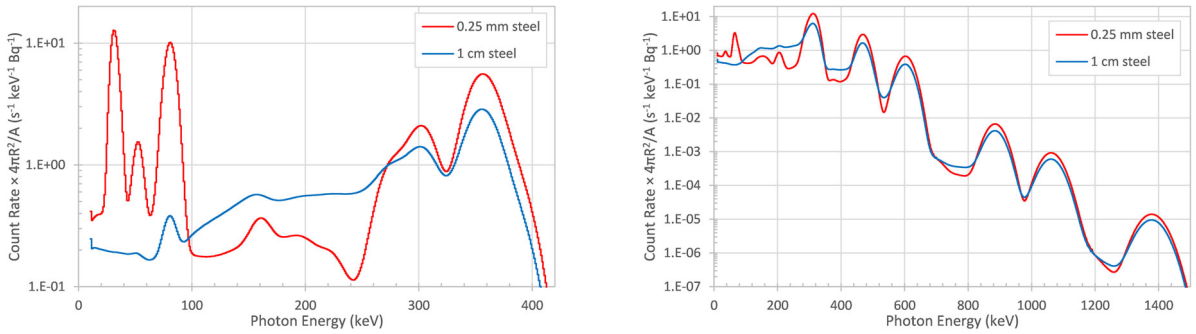

Figure 17. Predicted NaI count rate spectra for (left) ^{133}Ba and (right) ^{192}Ir. Red lines represent bare sources (with 0.25 mm steel), and blue lines represent sources shielded with 1 cm steel.

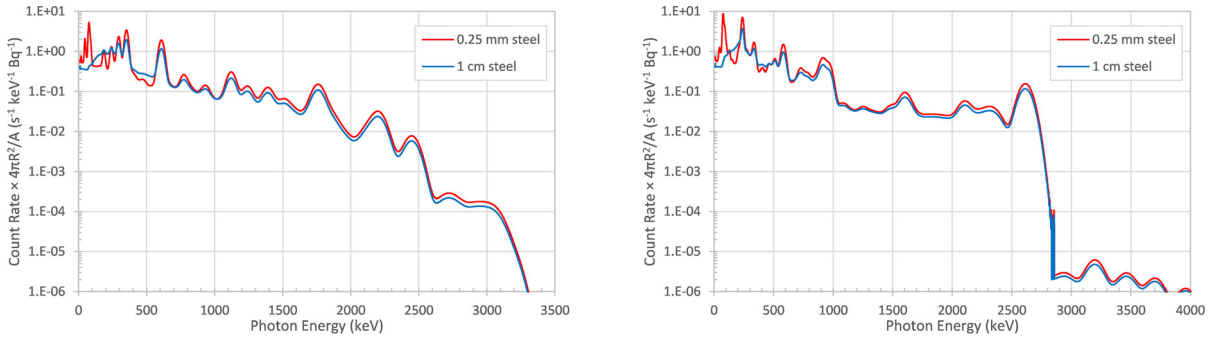

Figure 18. Predicted NaI count rate spectra for (left) ^{226}Ra and (right) ^{232}Th. Red lines represent bare sources (with 0.25 mm steel), and blue lines represent sources shielded with 1 cm steel.

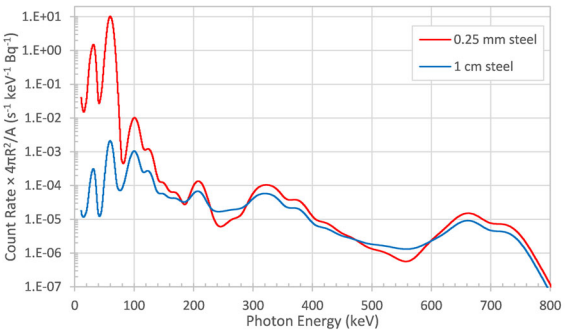

Figure 19. Predicted NaI count rate spectrum for ^{241}Am. The red line represent the bare sources (with 0.25 mm steel), and the blue line represents the source shielded with 1 cm steel.

2.6 BASIC SOURCES WITH POLYMETHYL METHACRYLATE

An Oak Ridge National Laboratory team working on the Wearable Intelligent Nuclear Detection project [10] [11] requested the creation of the basic sources with a shielding layer of 1.25 cm of polymethyl methacrylate (PMMA), also known as *plexiglass* or *Lucite*. PMMA has the chemical formula $(C_5H_8O_2)_n$ and a density of 1.19 g cm^{-3} [12]. The equivalent point source emission spectra for the basic isotopes with 1.25 cm of PMMA are shown in Figures 20–24. The predicted count rate for a NaI detector from each of the basic sources covered in PMMA are shown in Figures 25–29. Because PMMA consists of light elements, the count rates at the peak energies are attenuated only a small amount, and the amount of downscatter is larger compared with the same sources covered in 0.25 mm of steel. The uncertainties of the distributions using PMMA are less than the uncertainties when using 0.25 mm of steel but a bit larger than using 1 cm of steel.

Table 4 lists the isotopic photon emission strengths per unit activity and the corresponding strengths of the equivalent point sources, with shield layers of 0.25 mm of steel, 1 cm of steel, and 1.25 cm of PMMA.

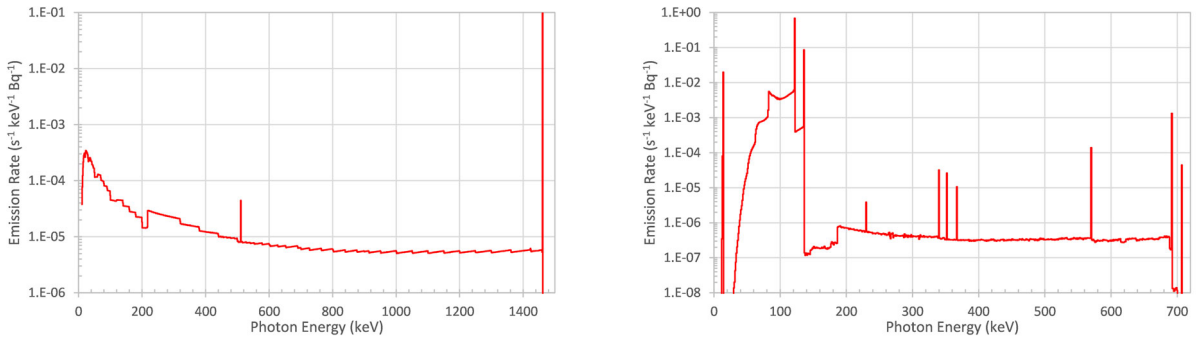

Figure 20. Equivalent point source emission spectra for (left) ^{40}K and (right) ^{57}Co shielded with PMMA.

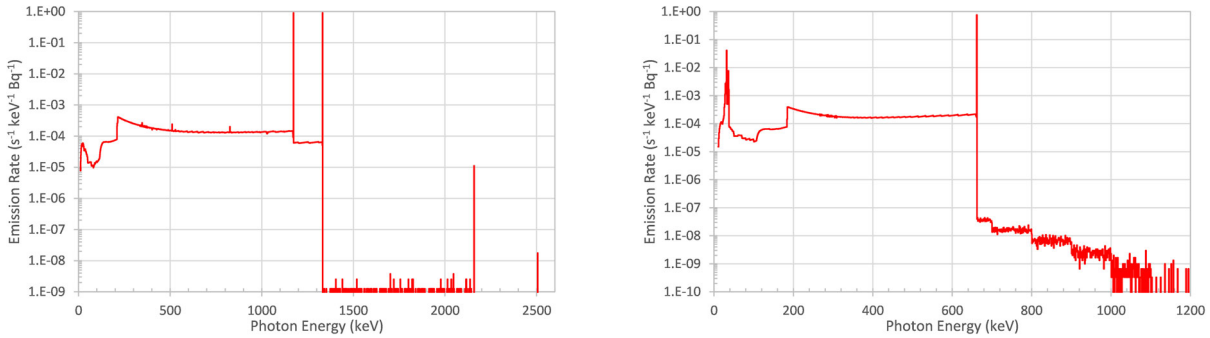

Figure 21. Equivalent point source emission spectra for (left) ^{60}Co and (right) ^{137}Cs shielded with PMMA.

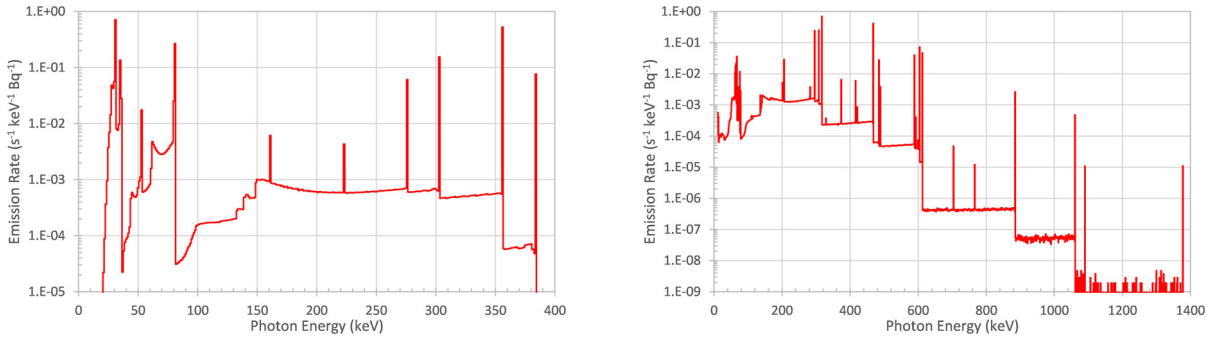

Figure 22. Equivalent point source emission spectra for (left) ^{133}Ba and (right) ^{192}Ir shielded with PMMA.

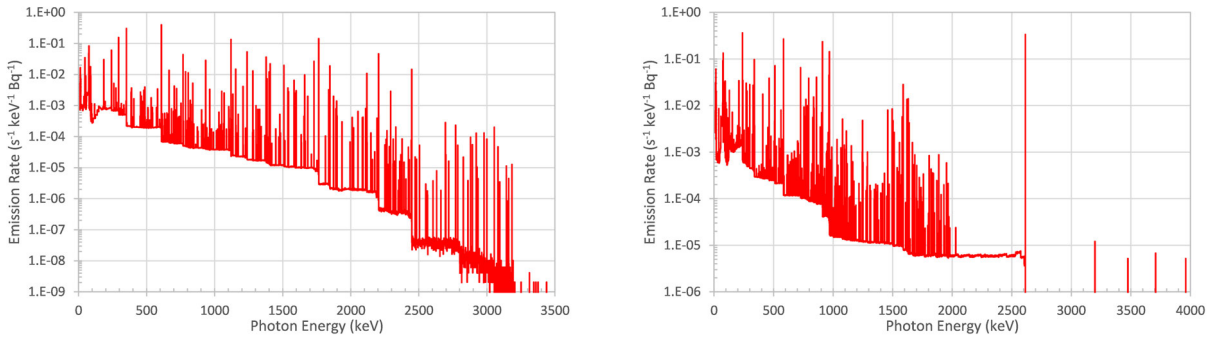

Figure 23. Equivalent point source emission spectra for (left) ^{226}Ra and (right) ^{232}Th shielded with PMMA.

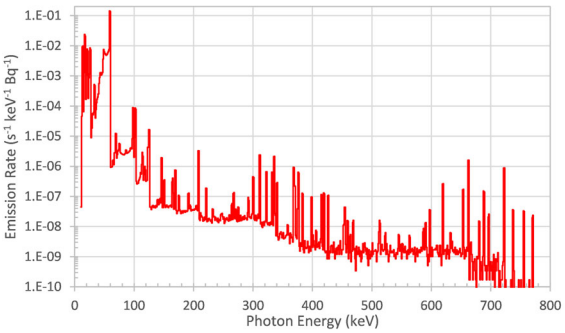

Figure 24. Equivalent point source emission spectra for ^{241}Am shielded with PMMA.

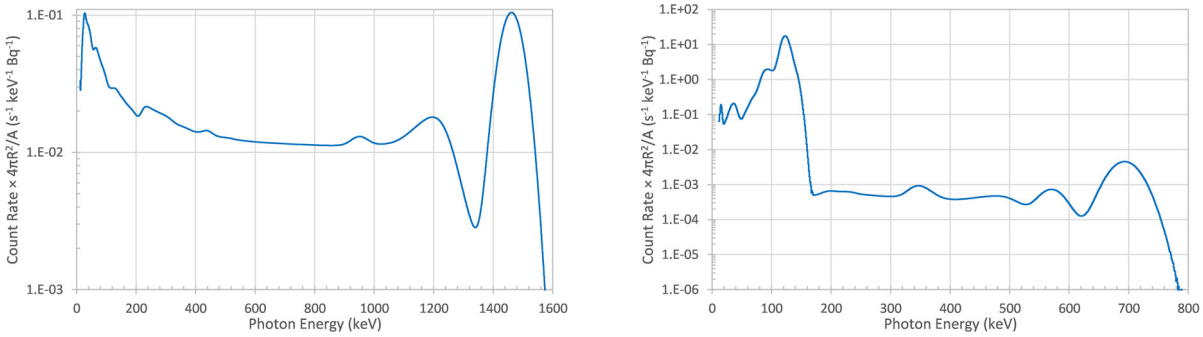

Figure 25. Predicted NaI count rate spectra for (left) ^{40}K and (right) ^{57}Co shielded with PMMA.

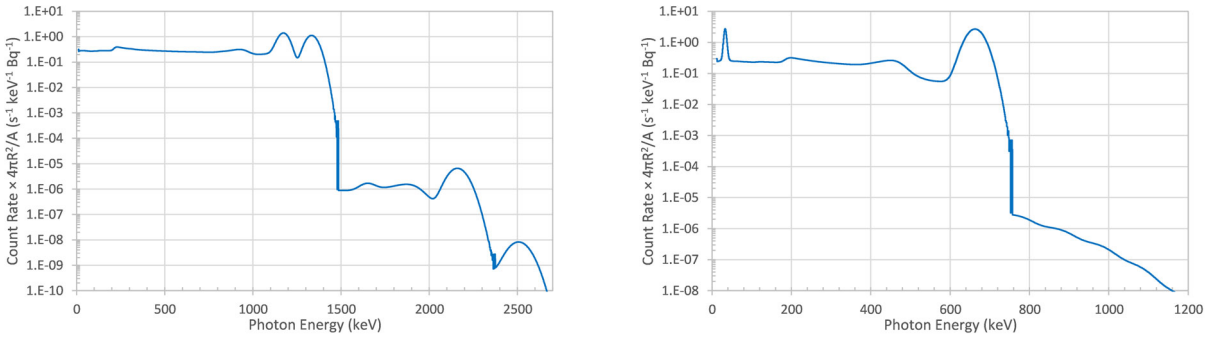

Figure 26. Predicted NaI count rate spectra for (left) ^{60}Co and (right) ^{137}Cs shielded with PMMA.

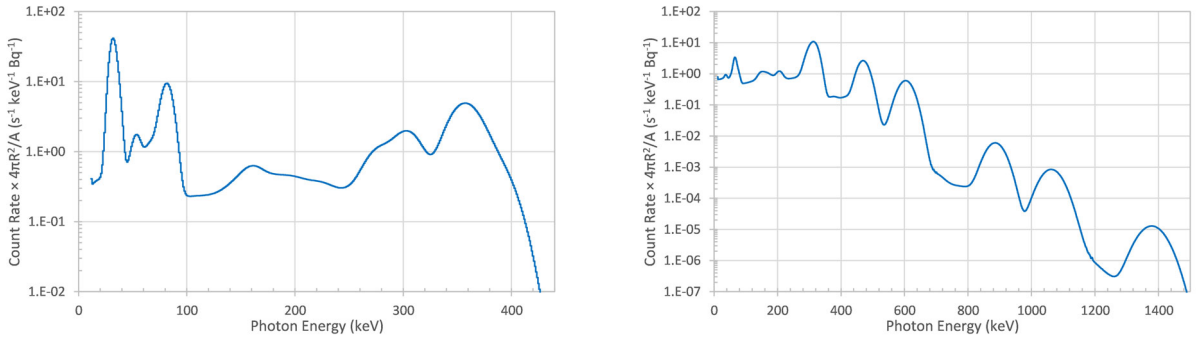

Figure 27. Predicted NaI count rate spectra for (left) ^{133}Ba and (right) ^{192}Ir shielded with PMMA.

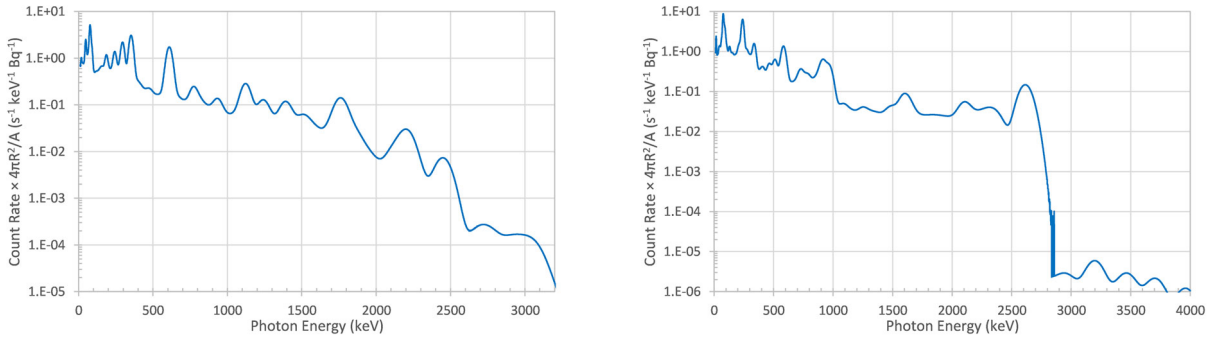

Figure 28. Predicted NaI count rate spectra for (left) ^{226}Ra and (right) ^{232}Th shielded with PMMA.

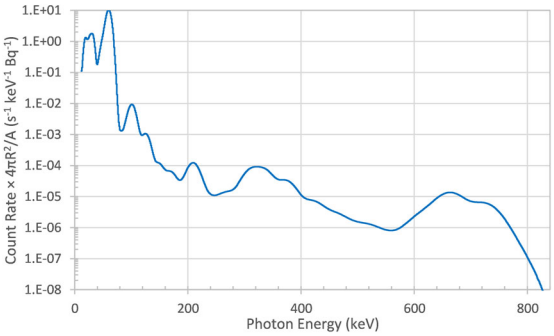

Figure 29. Predicted NaI count rate spectra for ^{241}Am shielded with PMMA.

Table 4. Emission strengths and equivalent point source strengths of the basic isotopes

Isotope	ORIGEN emission strength (s^{-1} Bq^{-1})	Equivalent point source strength* MAVRIC		
		0.25 mm steel (s^{-1} Bq^{-1})	1 cm steel (s^{-1} Bq^{-1})	1.25 cm PMMA (s^{-1} Bq^{-1})
^{40}K	0.133734	0.119157	0.104656	0.126370
^{57}Co	1.05618	0.942947	0.23287	0.983013
^{60}Co	2.00202	1.99934	1.88650	2.00066
^{137}Cs	0.928367	0.875157	0.762369	0.918110
^{133}Ba	2.58627	1.65825	0.763162	2.43615
^{192}Ir	2.33072	2.28253	1.69841	2.30480
^{226}Ra	2.71662	2.29412	1.75152	2.38215
^{232}Th	3.96158	3.06902	2.18930	3.29659
^{241}Am	0.636863	0.298849	0.000153	0.454576

*Uncertainties for 0.25 mm of steel are all <0.0025%. For 1 cm of steel, uncertainties are all <0.0035%, except ^{241}Am which was 0.01%. PMMA uncertainties are <0.0015%.

3. MEDICAL SOURCES

3.1 SOURCES LISTED IN THE N42 STANDARDS

The N42 standards discuss several medical sources, which are listed in Table 5. Table 6 lists additional information from other references on the levels of expected contaminants in these medical sources.

Table 5. Medical sources listed in the N42 standards

Isotope	Half-life	Comments
^{67}Ga	3.261 days	2–5 mCi
^{99m}Tc	6.01 h	3–25 mCi (possible ^{99}Mo impurity with 2.7476 days)
^{131}I	8.02 days	10–30 μCi and 29–300 mCi (diagnostics versus therapy)
^{201}Tl	3.039 days	4 mCi (sometimes contains ^{202}Tl with 12.23 days)

Table 6. Contaminants in medical sources

Isotope	Contaminants
^{67}Ga	The World Health Organization [13] reports that "not less than 99% of the total radioactivity is due to ^{67}Ga, and not more than 0.2% of the total radioactivity is due to ^{66}Ga." Other contributors to the total radioactivity were not listed. Drugs.com [14] reports that "at the time of calibration, the drug contains no more than 0.02% ^{66}Ga and no more than 0.2% ^{65}Zn."
^{99m}Tc	The International Atomic Energy Agency [15] reports that "the final radiopharmaceutical at the time of administration will not contain more than 0.15 KBq of ^{99}Mo per MBq of ^{99m}Tc (0.15 μCi of ^{99}Mo per mCi) at the time of administration."
^{131}I	The European Pharmacopoeia [16] states that a minimum of 99.9% of the total radioactivity is ^{131}I but could contain ^{130}I, ^{133}I, ^{135}I, and other radionuclidic impurities.
^{201}Tl	One manufacturer [17] says that the maximal contamination of ^{201}Tl (73 h half-life) could be 0.3% ^{200}Tl (368 and 579 keV; 26.1 h), 1.2% ^{202}Tl (439 keV;12.23 days), and 0.2% ^{203}Pb (258, 635, and 839 keV; 51.87 h) at calibration time. Groppi et al. [18] report that ^{202}Tl could be between 0.5% and 5%.

3.2 DEVELOPING SOURCES FOR RADAI/REX

To compute the x-ray and gamma-ray emission spectra with the SCALE/ORIGEN code, the contaminant amounts and a time after extraction must be specified so that the contributions from different radionuclides that decay and build up over time are properly weighted. Note that the discussion in this section does not include biological half-lives, which are different for each element and could also depend on what chemical compound contains the radionuclide.

The ^{67}Ga decays to a stable product, so without considering contaminants, the emission spectra distribution will not change over time; only the intensity will change. The contaminants ^{66}Ga (9.5 h) and ^{65}Zn (243.8 days) tend to have many gamma lines of low intensity. In the period of 1–10 days, the emission spectrum does not appreciably change with time. An activity mixture of 98.78% ^{67}Ga, 0.02% ^{66}Ga, and 0.2% ^{65}Zn was used.

The ^{99m}Tc decays to ^{99}Tc, which has a very long half-life (231,000 years) and will only reach 3.2 nBq per becquerel of the original ^{99m}Tc. Thus, ^{99m}Tc essentially decays to a stable daughter. The ^{99}Mo contaminant has a half-life of 2.7476 days and becomes ^{99m}Tc by beta decay. This decay adds an x-ray bremsstrahlung

spectrum and many lines between 100 keV and 1 MeV, but they are all at a very low intensity because of the low amount of contaminant. Within the few days that the ^{99m}Tc treatment is in effect, the spectrum does not appreciably change with time. The activity mixture used was 99.985% ^{99m}Tc and 0.015% ^{99}Mo.

Medical ^{131}I is produced from the fission process. The ^{131}I decays to ^{131m}Xe (11.9 days), and then it decays to stable ^{131}Xe. The ^{131m}Xe gives extra lines at 30–35 keV and a low-probability line at 164 keV (less than 10^{-3} of the strength of the main 364.5 keV line from ^{131}I). All the contaminants have shorter half-lives, and if the patient does not receive the treatment until a week after extraction, then the contaminant activities are reduced further by a factor of more than 100. An activity mixture of 99.9% ^{131}I and 0.0333% each of ^{130}I, ^{133}I, and ^{135}I was used.

The ^{201}Tl decays to a stable product, and the contaminants have a range of half-lives. Over the first week, only the 439 keV line from the ^{202}Tl changes, increasing from 0% to 5% of the emitted photons. This increase is because the other isotopes are decaying faster than the ^{202}Tl, so its gamma rays become more important. The total emission spectra from medical ^{201}Tl depends somewhat on time. The activity mixture used was 98.3% ^{201}Tl with 0.3% ^{200}Tl, 1.2% ^{202}Tl, and 0.2% ^{203}Pb.

The emission spectra of these medical isotopes computed using ORIGEN all included bremsstrahlung from beta radiation (using water as the slowing-down medium).

3.3 ADDITIONAL MEDICAL SOURCES

Scientists from the Detection Radiation Algorithms Group (DRAG) [19] suggested adding other medical sources that are occasionally encountered in urban searches but are not listed in the N42 standards. DRAG requested ^{133}Xe and ^{177}Lu be added as sources.

Radioactive ^{133}Xe has a half-life of 5.243 days and is used in lung diagnostic studies. A manufacturer [20] lists the composition of the Xe gas at 7 days after calibration as having an activity breakdown as >97.2% ^{133}Xe, <0.08% ^{133m}Xe, <2.5% ^{131m}Xe, <0.15% ^{85}Kr, and <0.02 ^{131}I. For this project, the maximum amounts of contaminants at 7 days were used. Amounts listed for total activities used in treatments ranged from 10 to 30 mCi.

Kuznetsov [21] says, “The main methods for producing ^{177}Lu of high specific activity are based on irradiation of either ^{176}Lu or ^{176}Yb with reactor neutrons [reactions ^{176}Lu(n,γ)^{177}Lu and ^{176}Yb(n,γ)^{177}Yb (β^--decay) → ^{177}Lu, respectively].” In either case, both ^{177}Lu and^{177m}Lu are made, as well as other isotopes. The Lu is synthesized into the final radiopharmaceutical, leaving any radioactive isotopes of non-Lu elements behind. The half-lives of ^{177}Lu and ^{177m}Lu are 6.647 days and 160.4 days, respectively. A few simple simulations of the activation of Lu in different thermal fluxes followed by a decay of one week gave an activity ratio of ^{177m}Lu/^{177}Lu of around 2×10^{-4}. For the activation and decay of Yb, the ratio of ^{177m}Lu/^{177}Lu was much lower—around 5×10^{-6}. For the Lu source in this project, a value of 2×10^{-4} for the ^{177m}Lu/^{177} ratio was used.

3.4 CALCULATED EMISSION SPECTRA

Emission spectra from the medical sources from ORIGEN are shown (using both linear and logarithmic axes) in Figures 30–35. Like the previous basic isotopic sources, each of these sources contains two plots: one with a linear vertical axis (left) and one with a logarithmic vertical axis (right).

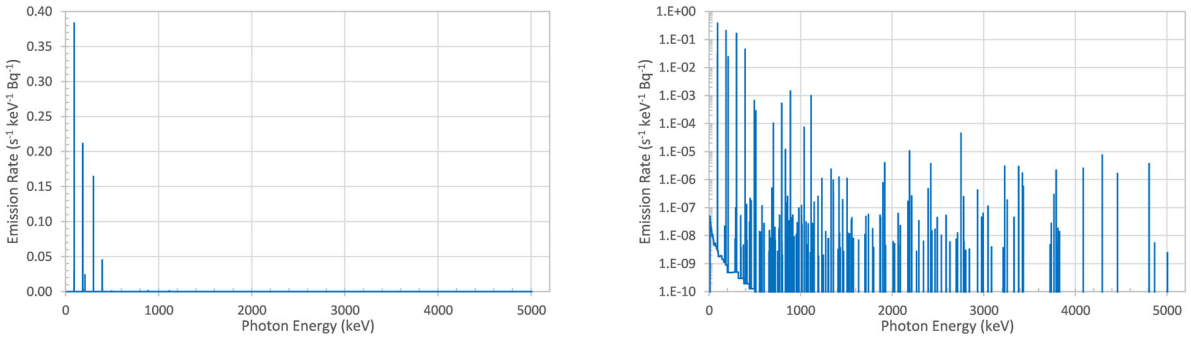

Figure 30. Emission spectrum for ^{67}Ga. (left) Linear vertical axis and (right) logarithmic vertical axis.

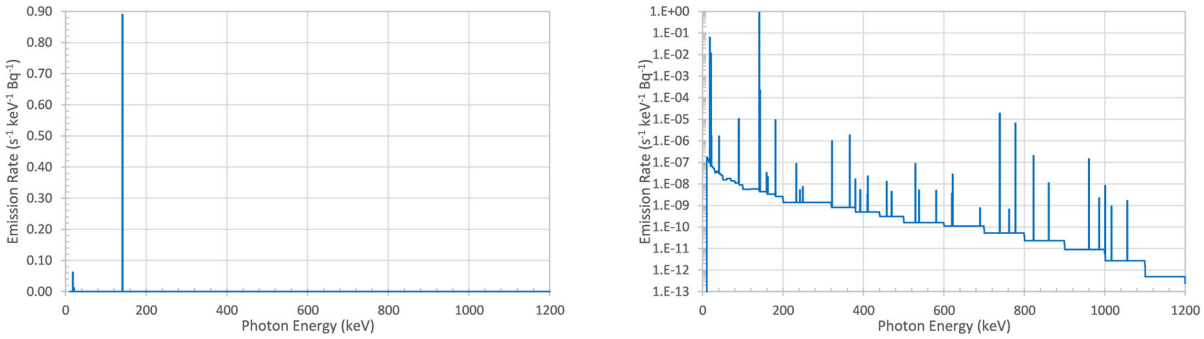

Figure 31. Emission spectrum for ^{99m}Tc. (left) Linear vertical axis and (right) logarithmic vertical axis.

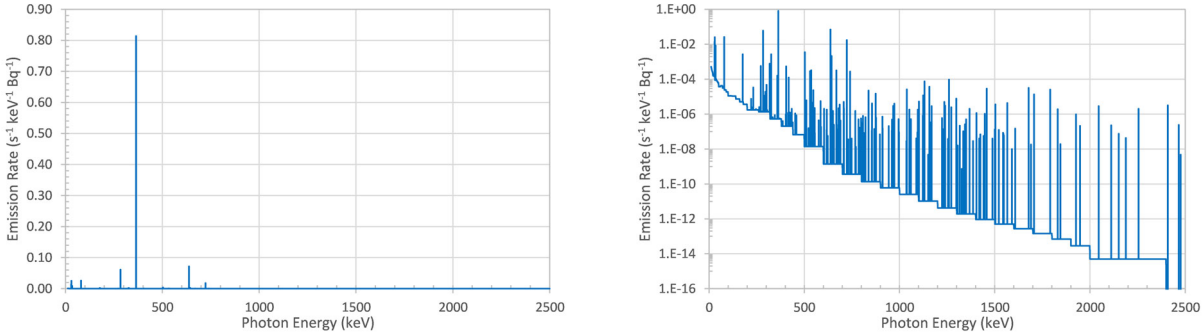

Figure 32. Emission spectrum for ^{131}I. (left) Linear vertical axis and (right) logarithmic vertical axis.

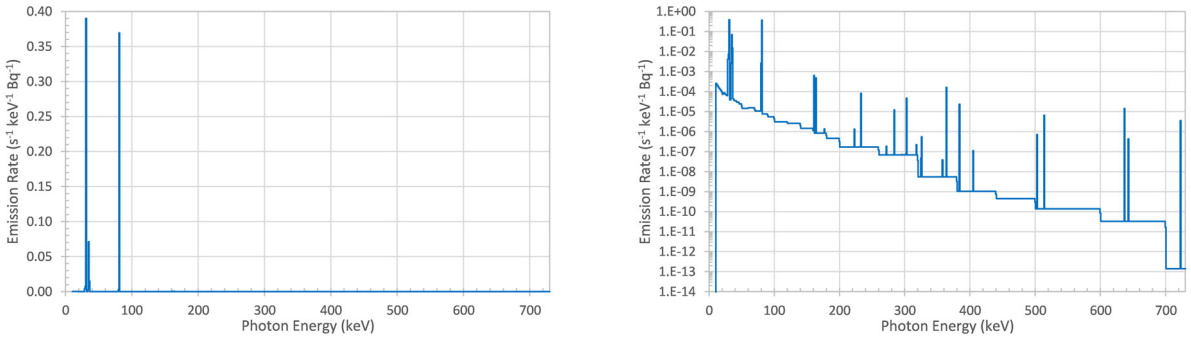

Figure 33. Emission spectrum for ^{133}Xe. (left) Linear vertical axis and (right) logarithmic vertical axis.

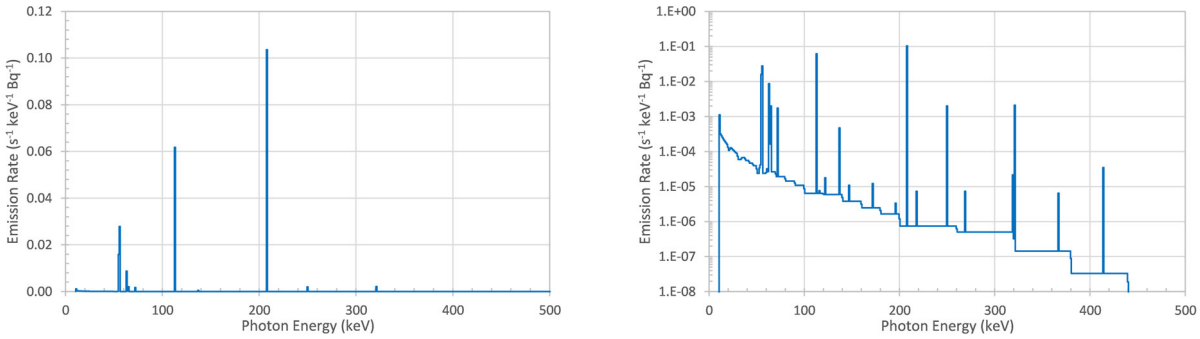

Figure 34. Emission spectrum for ^{177}Lu. (left) Linear vertical axis and (right) logarithmic vertical axis.

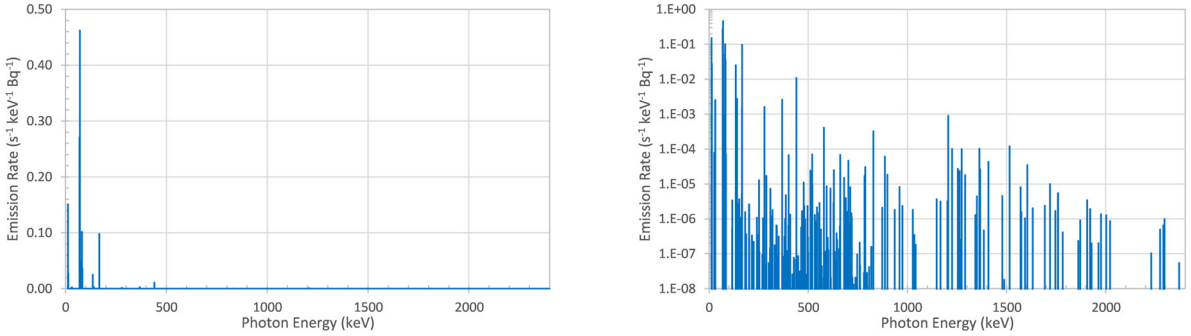

Figure 35. Emission spectrum for ^{201}Tl. (left) Linear vertical axis and (right) logarithmic vertical axis.

3.5 EQUIVALENT POINT SOURCE EMISSION SPECTRA

The emission spectra computed by ORIGEN were used in MAVRIC calculations to compute the flux escaping through 8 cm of PMMA per the N42 standards' recommendations for medical sources. These fluxes were also made into the equivalent point source emission spectra. Each medical isotope was modeled as point source in the center of a 1 cm radius void, which was inside a 9 cm radius sphere of PMMA. Figures 36–38 show the equivalent point source flux spectra, and Table 7 lists the emission strengths and the equivalent point source strengths of the medical isotopes considered here.

Relative uncertainties in the ^{76}Ga distribution are below 1% up to 400 keV, below 2% up to 495 keV, 3% up to 800 keV, and 6% up to 1,120 keV. Above 1,120 keV, the uncertainties are very large.

The ^{99m}Tc has uncertainties of 0.35% for energies between 50 and 141 keV, 8% from 141 to 181 keV, and from 13% to 25% from 181 to 739 keV. Above 739 keV, uncertainties are poor.

The I distribution has uncertainties 0.1% up to 364 keV, 0.4% up to 638 keV, 1% up to 723 keV, 10% below 1,000 keV, and 10%–15% up to 1,260 keV. Above 1,260 keV, uncertainties are very large.

The Xe uncertainties are 0.05% up to 81 keV, 1% up to 165 keV, 2%–4% up to 234 keV, 10% up to 385 keV, and 15%–25% up to 638 keV. Uncertainties are poor above 638 keV.

Uncertainties in the Lu distribution are 0.05% below 209 keV, 0.4%–0.6% up to 321 keV, 3%–5% up to 414 keV, and 10% up to 440 keV. Uncertainties increase quickly for energies greater than 440 keV.

The ^{201}Tl distribution has uncertainties of less than 0.2% below 167 keV, less than 1% up to 440 keV, 3% up to 579 keV, 4% up to 828 keV, 5% up to 1,206 keV, and then a steady increase from 10% above 1,206 keV to 25% at 1,516 keV.

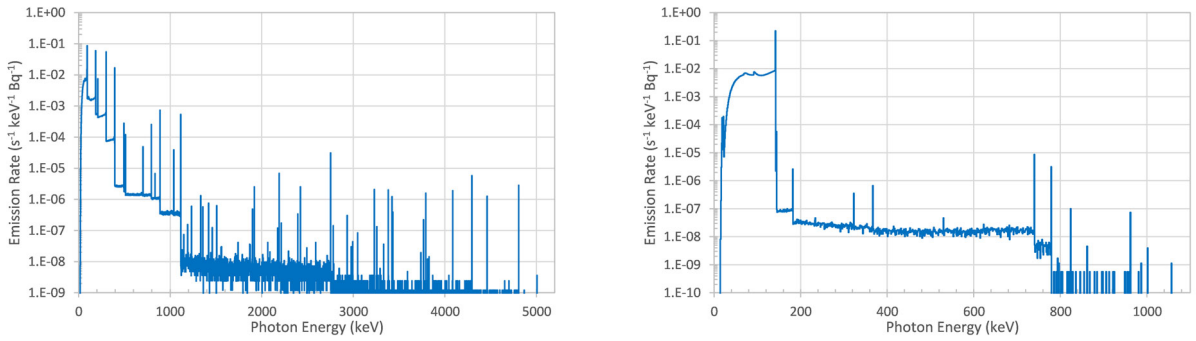

Figure 36. Equivalent point source emission spectra for (left) ^{67}Ga and (right) ^{99m}Tc.

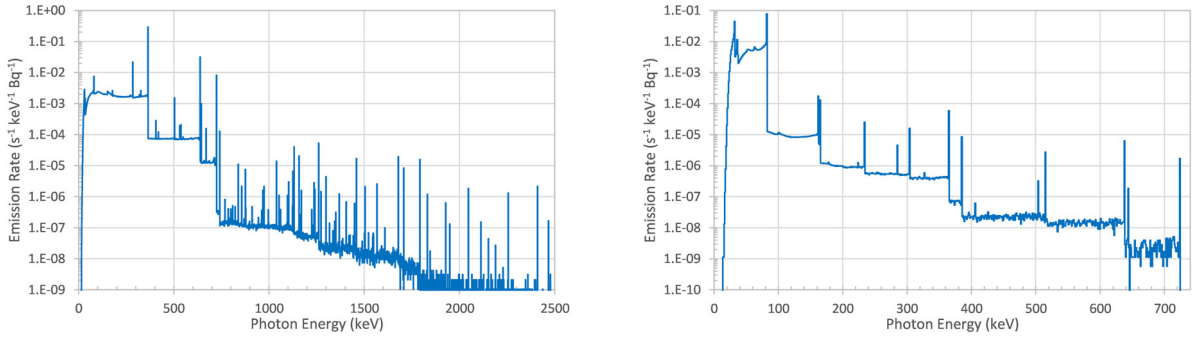

Figure 37. Equivalent point source emission spectra for (left) ^{131}I and (right) ^{133}Xe.

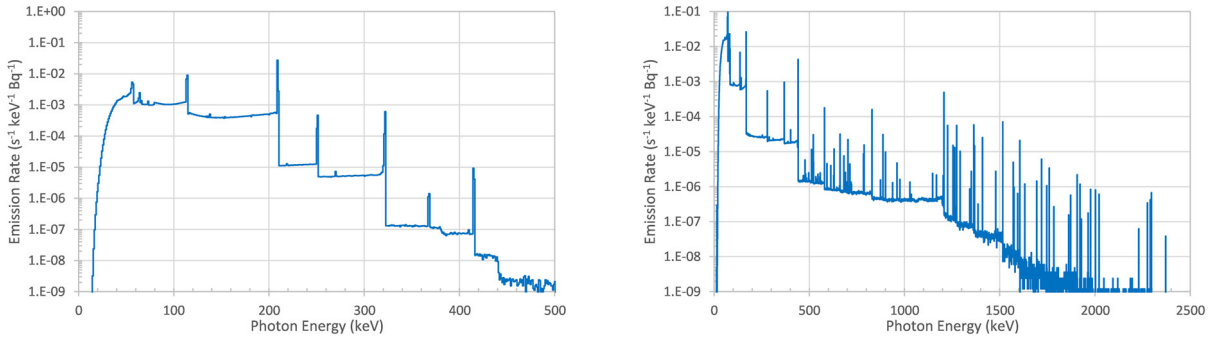

Figure 38. Equivalent point source emission spectra for (left) ^{177}Lu and (right) ^{201}Tl.

Table 7. Emission strengths and equivalent point source strengths of the medical isotope sources

Isotope	Emission strength ORIGEN (s^{-1} Bq^{-1})	Equivalent point source strength* MAVRIC (s^{-1} Bq^{-1})
^{67}Ga	0.863538	0.801227
^{99m}Tc	0.963795	0.839134
^{131}I	1.06283	1.00158
^{133}Xe	0.867386	0.439636
^{177}Lu	0.232994	0.202756
^{201}Tl	1.25330	0.885541

*Uncertainties are less than 0.0025%.

3.6 ESTIMATED SODIUM IODIDE DETECTOR RESPONSES

The 2 × 4 × 16 in. NaI detector response was combined with the energy-dependent fluxes to predict the NaI detector count rate. Figures 39–41 show the predicted count rate spectra in units of counts per second-kiloelectron volt-becquerel.

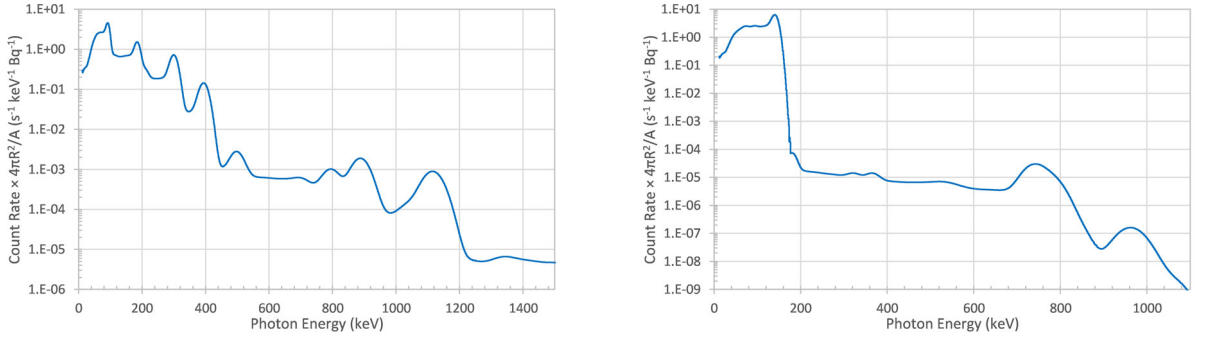

Figure 39. Predicted NaI count rate spectra for (left) ^{67}Ga and (right) ^{99m}Tc.

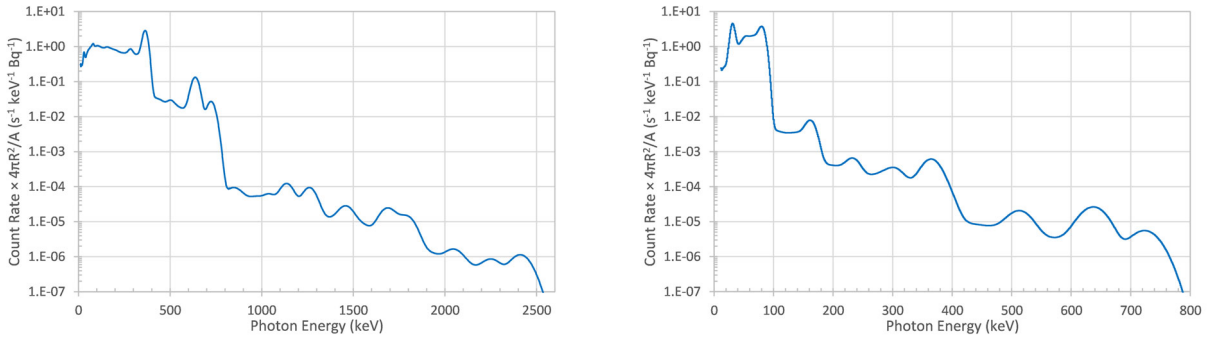

Figure 40. Predicted NaI count rate spectra for (left) ^{131}I and (right) ^{133}Xe.

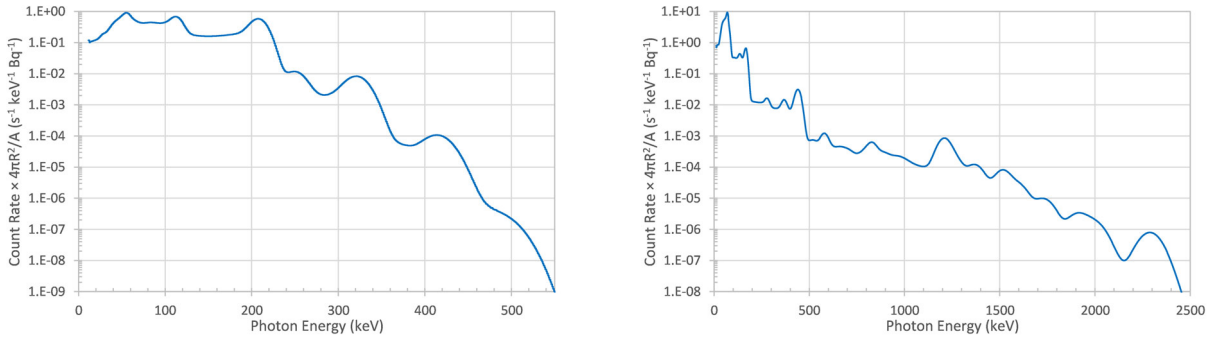

Figure 41. Predicted NaI count rate spectra for (left) ^{177}Lu and (right) ^{201}Tl.

Because none of the medical sources discussed here were positron emitters that would give 511 keV annihilation gamma rays, a pure 511 keV was also modeled in a 1 cm void inside of a 9 cm sphere of PMMA. The emission rate was based on an activity of 1 Bq of ^{18}F (which has a half-life of 110 min; 96.73% of decays give stable ^{18}O by positron emission, which emits two gamma rays at 511 keV) with no radioactive impurities. Only the annihilation gamma rays were considered—no bremsstrahlung was included. The equivalent point source flux spectra and predicted NaI count rate spectra for this pure 511 keV emitter are both shown in Figure 42. The emission strength of this emitter is 1.93460 s^{-1} Bq^{-1}, and the strength of the equivalent point source in 8 cm of PMMA is 1.91644 s^{-1} Bq^{-1}. Uncertainties for the equivalent point source are less than 0.07% between 50 and 511 keV.

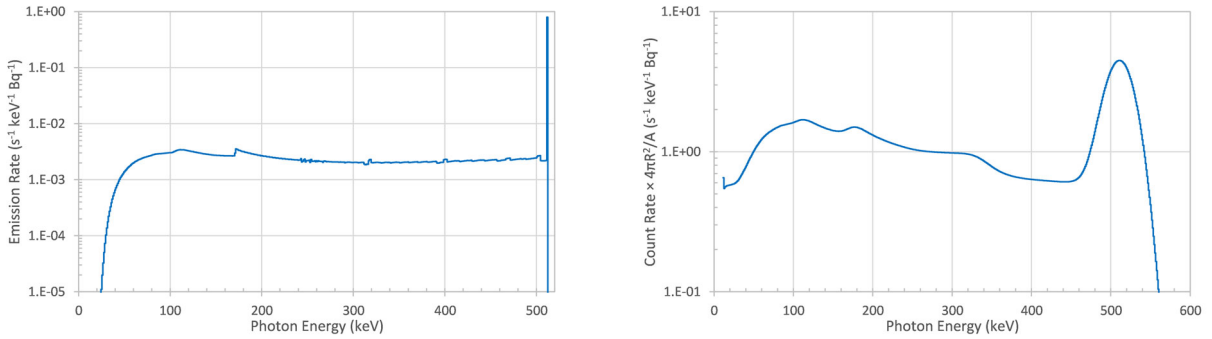

Figure 42. (left) Equivalent point source emission spectra and (right) predicted NaI count rate spectra for a pure 511 keV emmitter.

4. INDUSTRIAL SOURCES

DRAG also requested the creation of several shielded industrial sources that are occasionally encountered in urban searches. These sources included ^{67}Cu, ^{90}Sr, and ^{192}Ir with typical metal shielding as well as ^{192}Ir shielded with different thicknesses of depleted U (DU).

4.1 DEVELOPING SOURCES FOR RADAI/REX

The isotope ^{67}Cu has a half-life of 61.83 h and emits both gamma and beta radiation. The gamma rays are all under 400 keV. The decay product is stable ^{67}Zn. This isotope was processed in the same way as the RADAI basic isotopic sources: ORIGEN was used to create a source distribution for the photons, using the choice of water for the bremsstrahlung creation from the beta particles.

The isotope ^{90}Sr has a half-life of 28.91 years and only decays by beta emission (end-point energy 545.9 keV), resulting in ^{90}Y, which has a half-life of 64.05 h and decays by beta emission (99.9885% of decays are beta emissions with an end-point energy of 2,278.5 keV). Figure 43 shows the beta particle energy distribution for ^{90}Sr/^{90}Y from ORIGEN. Some x-rays (15–18 keV) are also emitted (<0.01% of decays) as well as a rare 2,186.242 keV gamma ray that is emitted 14 times per billion decays. Because of their low energies or very low probabilities, the photons were ignored. The MC N-Particle (MCNP) code [22] was used to transport ^{90}Sr/^{90}Y beta particles and generate bremsstrahlung in Al shells of thicknesses 1 and 2 cm. The beta particles were stopped within the first 0.6 cm of the Al spherical shell casing. MCNP was used for bremsstrahlung generation because the ORIGEN choices for a slowing-down medium do not include Al.

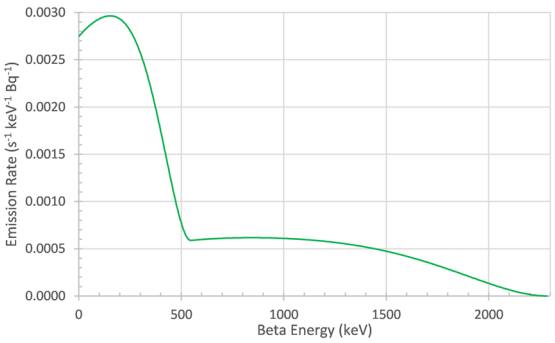

Figure 43. ^{90}Sr/^{90}Y beta spectra from ORIGEN.

Shielded ^{192}Ir was chosen as an example of industrial radiography sources that could be encountered in urban searches. The half-life of ^{192}Ir is 73.829 days, and it decays to stable ^{192}Pt by beta emission (95.24%, with the highest end-point energy of 670 keV) and gamma emission. The isotope ^{192}Ir also decays by electron capture (4.76%) to stable Os^{192}. The emission spectrum was computed using ORIGEN, with water as the bremsstrahlung option.

Using DU as a shield is interesting because being a dense and high-*Z* material, it is very effective. But, the DU shield will act a source itself. Enghauser [23] lists the isotopic breakdown of DU as 0.001% ^{234}U, 0.1995% ^{235}U, and 99.7995% ^{238}U. ORIGEN was used to compute the emission spectra of this mixture, aged 1 year to allow the daughter products to build in and using the UO_2 option for bremsstrahlung creation.

4.2 CALCULATED EMISSION SPECTRA

The photon emission spectrum for ^{67}Cu, ^{192}Ir, and DU from ORIGEN are shown in Figures 44–46. Two plots are shown for each: one with a linear vertical axis (left) and one with a logarithmic vertical axis (right).

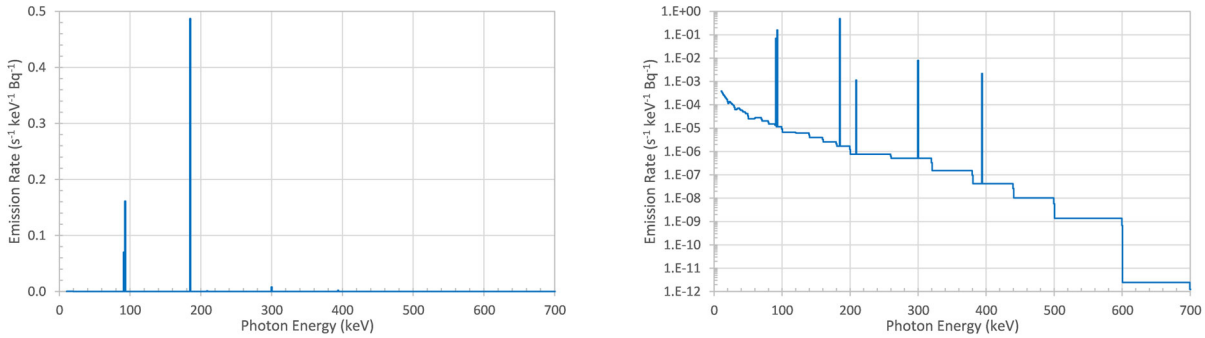

Figure 44. ^{67}Cu photon emission spectrum. (left) Linear vertical axis and (right) logarithmic vertical axis.

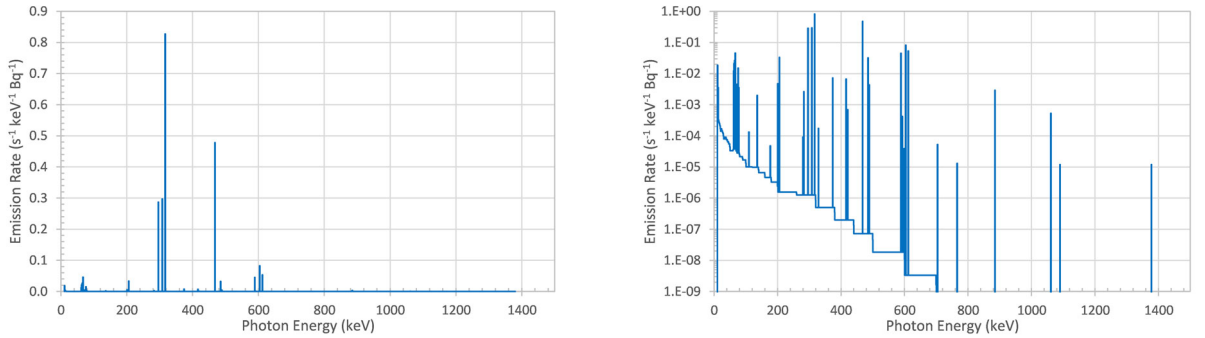

Figure 45. ^{192}Ir photon emission spectra. (left) Linear vertical axis and (right) logarithmic vertical axis.

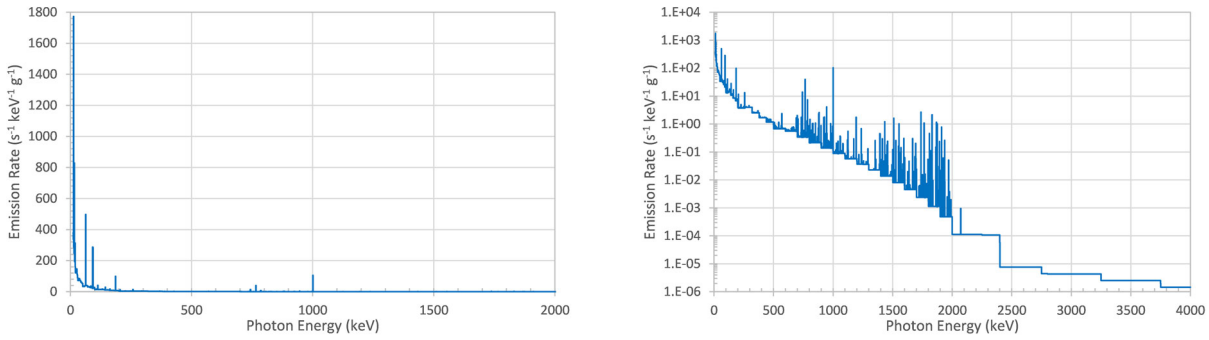

Figure 46. DU photon emission spectra. (left) Linear vertical axis and (right) logarithmic vertical axis.

4.3 EQUIVALENT POINT SOURCE EMISSION SPECTRA

For ^{67}Cu in steel (0.25 mm or 1 cm) and ^{192}Ir in thick steel (2 or 5 cm), the equivalent point source emission spectra were computed with MAVRIC using the ORIGEN sources. For ^{90}Sr/^{90}Y in Al (1 or

2 cm), the ORIGEN betas were used in MCNP to generate the equivalent point source emission spectra. The spectra are shown in Figures 47 and 48.

Uncertainties in the distribution for ^{67}Cu with 0.25 mm of steel are less than 0.3% from 93 to 185 keV, 0.9%–1.2% from 185 to 300 keV, 1.8%–4% up to 395 keV, 8% up to 441 keV, and 15% up to 500 keV. With 1 cm of steel, the uncertainties are 0.1% from 93 to 185 keV, 0.4% from 185 to 300 keV, 1% up to 395 keV, 11%–13% up to 441 keV, and 20%–25% up to 500 keV.

The uncertainties for the ^{90}Sr/^{90}Y sources in either 1 or 2 cm of Al are similar. From 100 to 500 keV, the uncertainty rises from 0.5% to 2.3%, to 6.5% at 1,000 keV, and to 20% at 1,500 keV.

The ^{192}Ir source in 2 cm of steel has relative uncertainties of 0.1% from 100 to 317 keV, 0.13% to 468 keV, 0.3% to 590 keV, 3% to 885 keV, and 8%–9% up to 1,061 keV. With 5 cm of steel, uncertainties are 0.15% from 160 to 317 keV, 0.25% to 468 keV, 0.5% to 590 keV, 4.5% to 885 keV, and 12% up to 1,061 keV.

The point source emissions from ^{192}Ir encased in DU have relative uncertainties similar to the Ir in steel except that the lower photon energies (<500 keV) are more severely attenuated by DU and therefore have much higher uncertainties.

The five shells of DU have similar relative uncertainties to one another, with the 5 mm shell having the lowest and the 30 mm shell having the highest. Uncertainties are 0.3%–0.7% from 100 to 1,000 keV, then up to 1.5%–2.5% by 1,500 keV and 9%–16% at 2,000 keV.

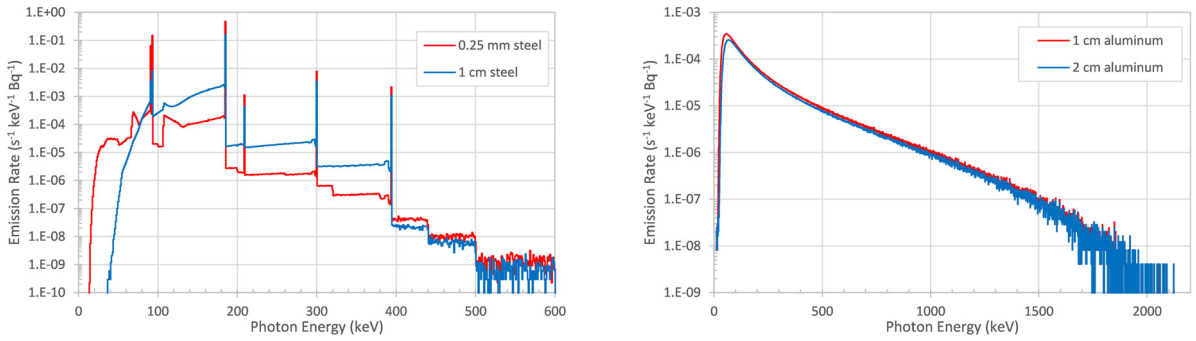

Figure 47. Equivalent point source emission spectra for (left) ^{67}Cu and (right) ^{90}Sr/^{90}Y.

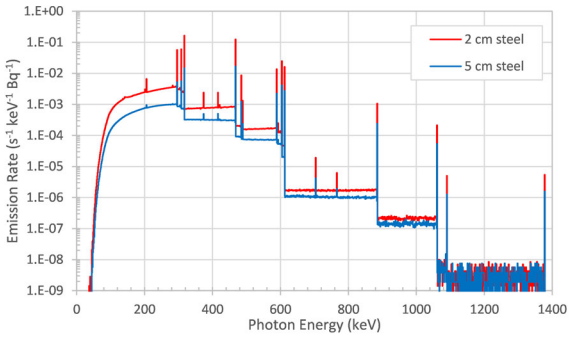

Figure 48. Equivalent point source emission spectrum for ^{192}Ir in steel.

The cases for Ir with DU shielding were done separately so that *any* strength of Ir could be combined with one of the modeled thicknesses of DU (5, 10, 15, 20, 25, and 30 mm). MAVRIC used the ORIGEN emission spectra for ^{192}Ir at 1 Bq and computed the equivalent point source emission spectra after passing through a given DU shell thickness. These spectra can be scaled to any strength of ^{192}Ir. MAVRIC was also used to compute the equivalent point source emission spectra for the six DU shells. The DU shells have fixed strengths that depend on the thickness, t, of the shell. The DU shell was modeled as a 1 cm inner radius void and an outer radius of t + 1 cm. The source strength of the shell is simply the product of volume of the shell, which is $(4\pi/3)[(t + 1\text{ cm})^3 - (1\text{ cm})^3]$, the density of DU (19.0 g cm^{-3}) and the DU emission strength. A simple linear combination of any strength of the ^{192}Ir equivalent point source emission spectra can be added to the equivalent point source emission spectra for the corresponding DU shell spectra. The components are shown in Figure 49. Table 8 shows the emission strengths and equivalent point source emission strengths of the industrial sources.

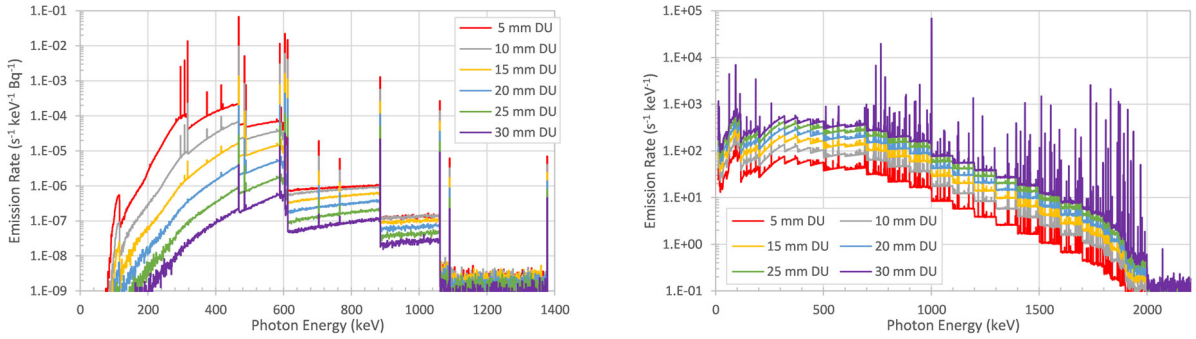

Figure 49. Equivalent point source emission spectra for ^{192}Ir inside shells of DU and (right) shells of DU.

Table 8. Emission strengths and equivalent point source strengths of the industrial sources

Isotope	Shielding	Emission strength ORIGEN (s^{-1} Bq^{-1})	Equivalent point source strength* MAVRIC (s^{-1} Bq^{-1})
^{67}Cu	0.25 mm steel	0.735518	0.715821
	1 cm steel		0.277583
$^{90}Sr/^{90}Y$	1 cm Al	1.9569†	0.0402390
	1 cm Al		0.0320195
^{192}Ir	2 cm steel	2.33072	1.13831
	5 cm steel		0.261631
^{192}Ir	in 5 mm DU	2.33072	0.177071
	in 10 mm DU		0.0340627
	in 15 mm DU		8.08905×10^{-3}
	in 20 mm DU		2.13554×10^{-3}
	in 25 mm DU		6.17508×10^{-4}
	in 30 mm DU		1.94995×10^{-4}
Depleted Uranium‡	5 mm thick spherical shell	2.34865×10^{6}	6.30920×10^{4}
	10 mm thick spherical shell	6.92234×10^{6}	1.20468×10^{5}
	15 mm thick spherical shell	1.44627×10^{7}	1.92414×10^{5}
	20 mm thick spherical shell	2.57116×10^{7}	2.80075×10^{5}
	25 mm thick spherical shell	4.14104×10^{7}	3.83671×10^{5}
	30 mm thick spherical shell	6.23011×10^{7}	5.03348×10^{5}

*Uncertainties on the point source equivalent strengths are less than 0.13%.
†ORIGEN emission strength for $^{90}Sr/^{90}Y$ is for beta radiation.
‡Strengths for DU are in units of s^{-1}.

4.4 ESTIMATED SODIUM IODIDE DETECTOR RESPONSES

The response of a 2 × 4 × 16 in. NaI detector was computed using the equivalent point source spectra to estimate the NaI detector count rate spectra. Figures 50–52 show the predicted count rates in units of counts per second-kiloelectron volt-becquerel for ^{67}Cu in steel, $^{90}Sr/^{90}Y$ in Al, and ^{192}Ir in steel. Count rates for ^{192}Ir inside DU shells are also in counts per second-kiloelectron volt-becquerel, but count rates of the DU shells are in counts per second-kiloelectron volt.

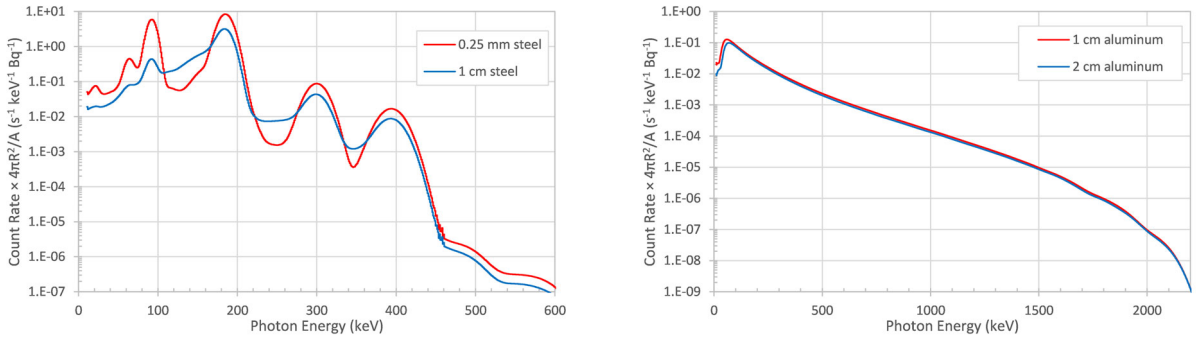

Figure 50. Predicted NaI count rate spectra for (left) ^{67}Cu and (right) $^{90}Sr/^{90}Y$.

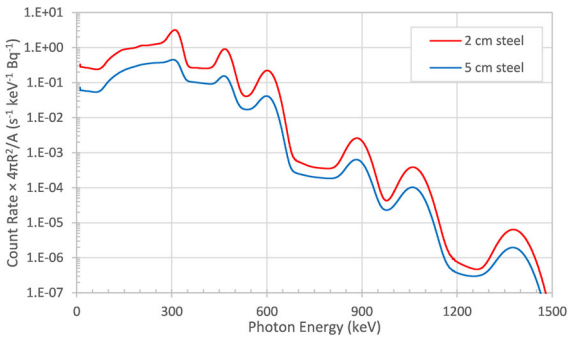

Figure 51. Predicted NaI count rate spectrum for ^{192}Ir in steel.

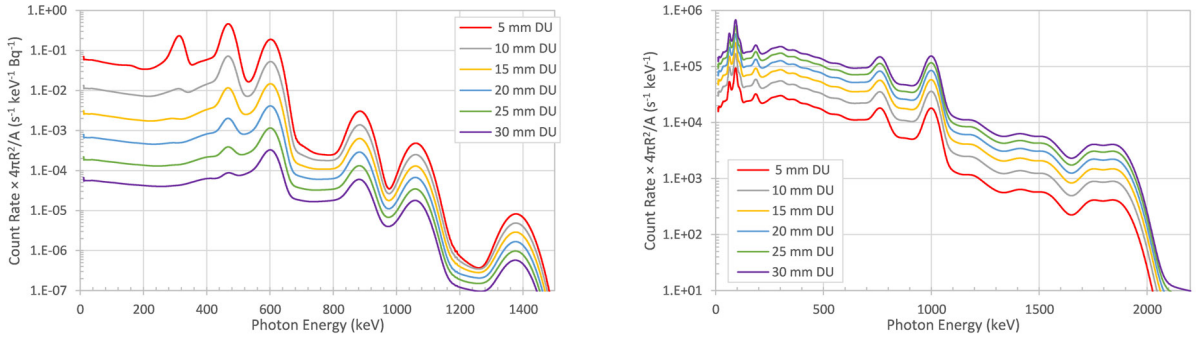

Figure 52. Predicted NaI count rate spectra for ^{192}Ir in (left) DU shells and (right) DU shells.

These ^{192}Ir and DU components would be used in the following way. First, the thickness of the DU shell is picked. Then the ^{192}Ir count rate spectrum is scaled by the desired Ir activity and is added to the count rate spectrum for the selected shell. Examples shown in Figure 53 are for the predicted NaI detector response for the 15 mm shell thickness of DU and various activities of Ir.

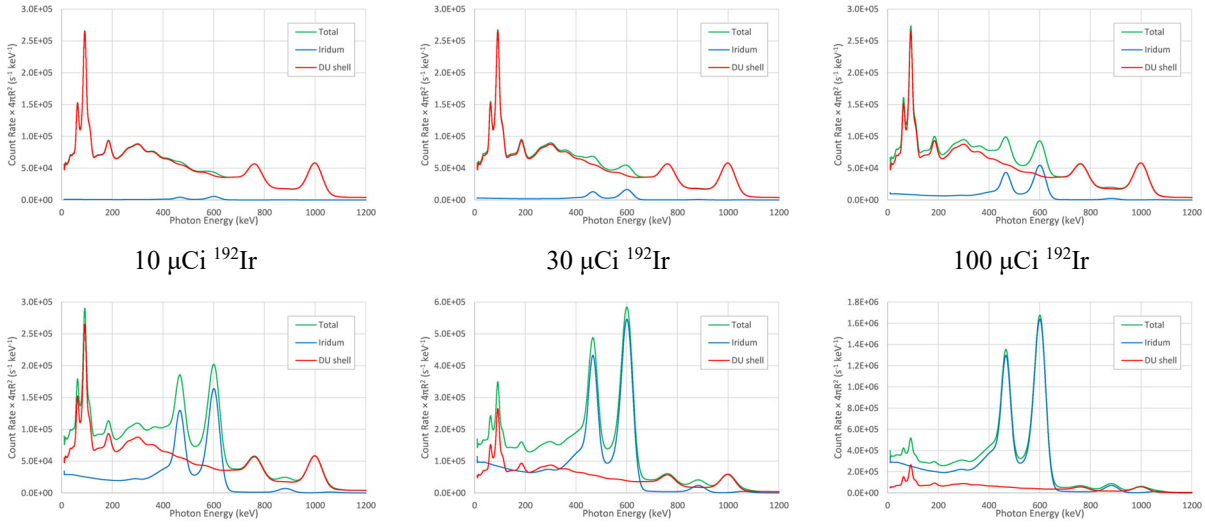

10 µCi ^{192}Ir | 30 µCi ^{192}Ir | 100 µCi ^{192}Ir

300 µCi ^{192}Ir | 1 mCi ^{192}Ir | 3 mCi ^{192}Ir

Figure 53. Predicted NaI count rate spectra for different activities of ^{192}Ir in a 15 mm shell of DU.

5. SPECIAL NUCLEAR MATERIAL

5.1 SOURCES LISTED IN THE N42 STANDARDS

The N42 standards list several different materials containing U and Pu but they do not completely specify the full isotopic composition. Materials include DU, low-enriched U (LEU), highly enriched U (HEU), reactor-grade Pu (RGPu), fuel-grade Pu (FGPu), and weapons-grade Pu (WGPu). These materials are listed in Table 9. Note that the different standards have slightly different compositions listed for WGPu.

Table 9. SNM sources list in the N42 standards

Material	Definition and comments
DU	<0.72% ^{235}U
U ore	Natural U, secular equilibrium
Refined U	Natural U, only short-lived ^{234}Th and ^{234m}Pa built in
LEU	≤20% ^{235}U
HEU	>20% ^{235}U, ≥90% ^{235}U
^{238}Pu	~90% ^{240}Pu + ^{238}Pu
RGPu	Primarily ^{239}Pu with ~15% ^{240}Pu
FGPu	(Primarily ^{239}Pu, with less than 6% ^{240}Pu) or (≤6.5% ^{240}Pu and >93% ^{239}Pu)
WGPu	Shielded to reduce ^{241}Am 60 keV line, Cu alloy, or Cd shielding

Enghauser [23] listed the isotopic compositions of different kinds of U. These compositions are shown in Table 10.

Table 10. Enghauser's typical U mass percentages

Nuclide	DU mass %	Natural U mass %	3% enriched mass %	93.3% enriched mass %
^{234}U	0.0010	0.0055	0.0268	0.8692
^{235}U	0.1995	0.7115	3.0000	93.3000
^{238}U	99.7995	99.2830	96.9732	5.8308

US Department of Energy (DOE) Standard 3013-2018 [24] contains isotopic amounts for WGPu, FGPu, and power-grade Pu (PGPu) just after discharge. This standard also contains isotopic amounts for aged Pu mixtures that include ^{241}Am. The isotopic compositions from Table B-10 of that standard are listed in Table 11. The report notes that the Hanford mixes have been aged for 10–30 years. Note that the weight fractions in that table are normalized such that the total Pu mass is 100%.

Table 11. Plutonium compositions from DOE Standard 3013-2018

Nuclide	Pure ^{239}Pu (%)	WGPu (%)	FGPu (%)	PGPu (%)	Hanford 4%–7% (%)	Hanford 10%–13% (%)	Hanford 16%–19% (%)
^{238}Pu	—	0.05	0.1	0.99	0.01	0.09	0.24
^{239}Pu	100.0	93.50	86.1	62.38	93.77	86.94	80.66
^{240}Pu	—	6.00	12.0	21.78	6.00	11.81	16.98
^{241}Pu	—	0.40	1.6	11.88	0.20	1.00	1.44
^{242}Pu	—	0.05	0.2	2.97	0.03	0.17	0.69
^{241}Am	—	—	—	—	0.14	0.86	2.80

5.2 DEVELOPING SOURCES FOR RADAI/REX

For the U compositions other than the natural U ore, the ORIGEN calculations started with Enghauser's compositions, and the materials were aged 1 year, allowing buildup of ^{234}Th, ^{234m}Pa, and ^{234}Pa from ^{238}U and ^{231}Th from ^{235}U. For the natural U ore, an initial composition was picked (0.57978 g ^{235}U and 1.98570 g ^{238}U) so that after aging one ^{238}U half-life, the amounts of ^{234}U, ^{235}U, and ^{238}U matched the masses for U found in nature (listed in Enghauser's table). This process allowed buildup of everything in the ^{235}U and ^{238}U decay chains down to Pb and assumed the gas isotopes of Rn stayed trapped within the ore.

The Pu isotopes have shorter half-lives than the U isotopes, particularly ^{241}Pu (14.4 years), which decays into ^{241}Am (432.7 years, 59.5 keV gamma rays). The Hanford mixes—which may represent averages of similar materials and do not show the amounts of daughter products other than ^{241}Am—were not used for developing any sources. For the different grades of Pu, the initial Pu isotopic compositions from DOE Standard 3013-2018 for WGPu, FGPu, and PGPu were used as the starting compositions. These were aged in ORIGEN for 20 years to allow daughters to build in. The gamma rays from Pu isotopes tend to have low emission rates per decay, so these materials may be difficult to differentiate from the basic isotopic source of ^{241}Am. With increased decay times, the ^{241}Am 59.54 keV gamma radiation becomes even stronger as more ^{241}Pu decays.

Information was not found on the impurities that would be in ^{238}Pu. This isotope was also aged for 20 years, allowing ^{234}U to build in.

5.3 CALCULATED EMISSION STRENGTH AND SPECTRA

The emission strengths and spectra of the SNM-related materials are shown in Figures 54–62. The spectra are shown using both a linear axis (left) and a logarithmic axis (right).

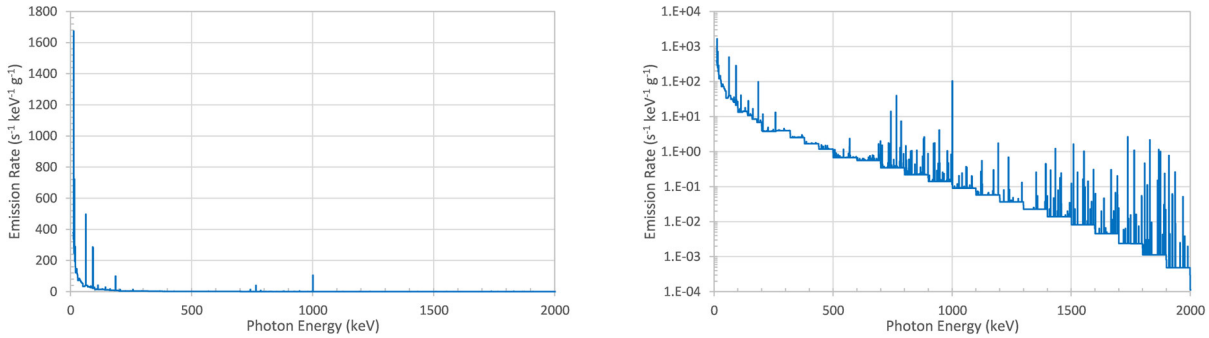

Figure 54. Emission spectrum for DU. (left) Linear vertical axis and (right) logarithmic vertical axis.

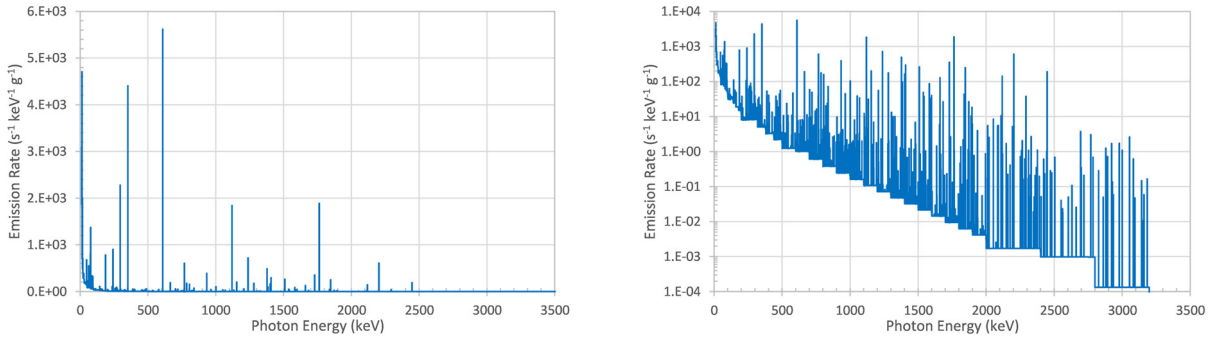

Figure 55. Emission spectrum for U ore. (left) Linear vertical axis and (right) logarithmic vertical axis.

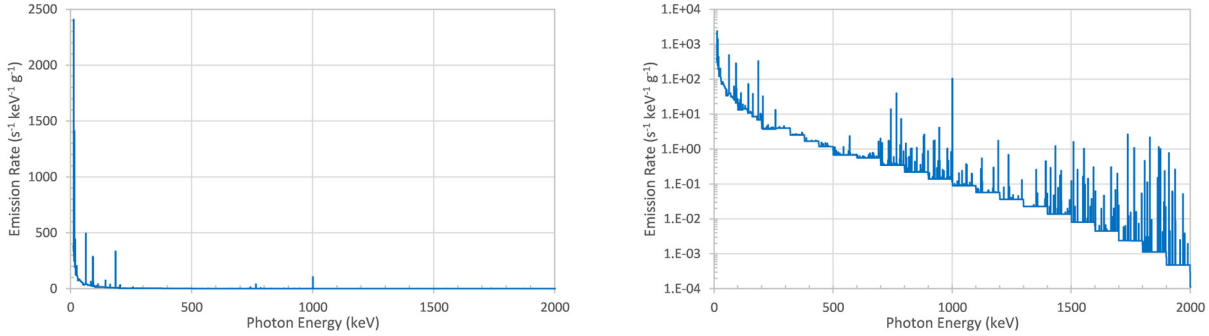

Figure 56. Emission spectrum for refined U. (left) Linear vertical axis and (right) logarithmic vertical axis.

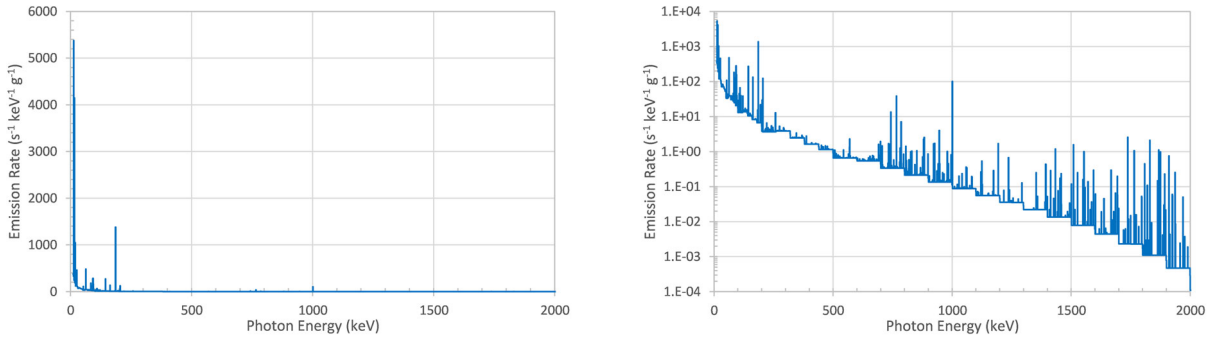

Figure 57. Emission spectrum for LEU. (left) Linear vertical axis and (right) logarithmic vertical axis.

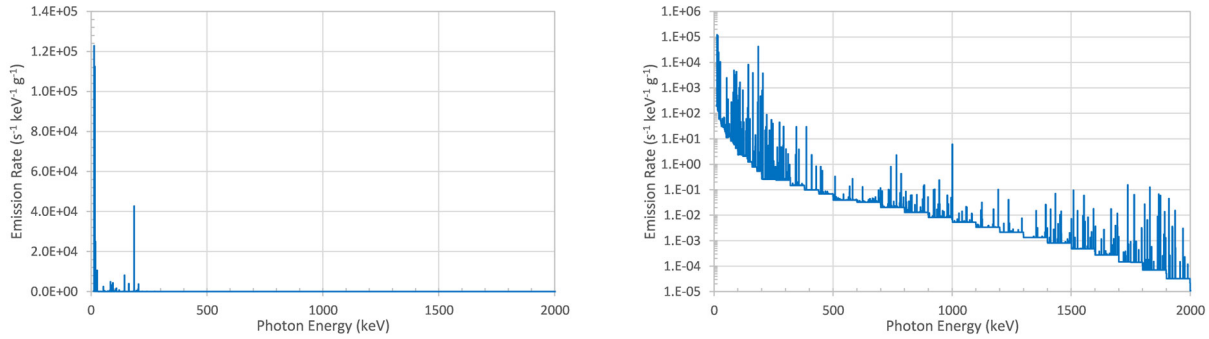

Figure 58. Emission spectrum for HEU. (left) Linear vertical axis and (right) logarithmic vertical axis.

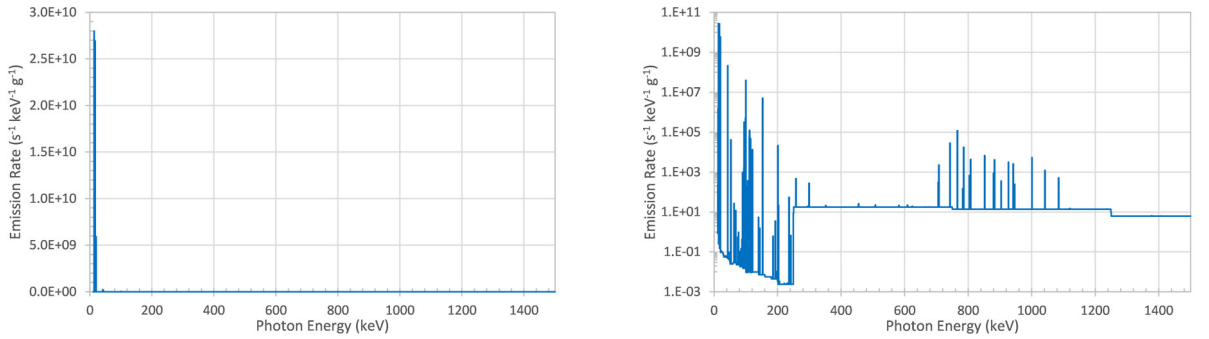

Figure 59. Emission spectrum for ^{238}Pu. (left) Linear vertical axis and (right) logarithmic vertical axis.

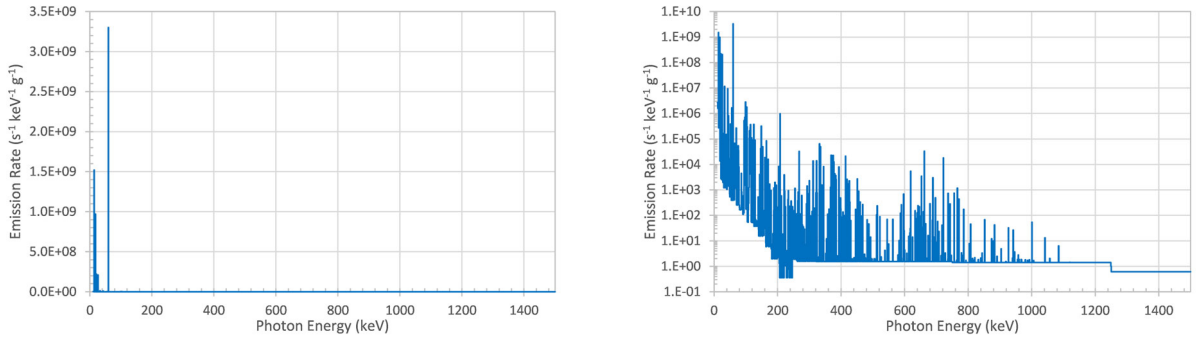

Figure 60. Emission spectrum for PGPu. (left) Linear vertical axis and (right) logarithmic vertical axis.

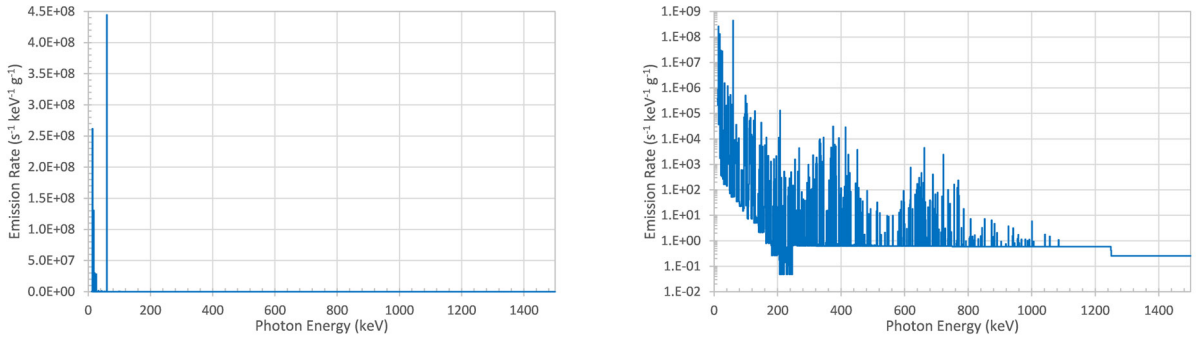

Figure 61. Emission spectrum for FGPu. (left) Linear vertical axis and (right) logarithmic vertical axis.

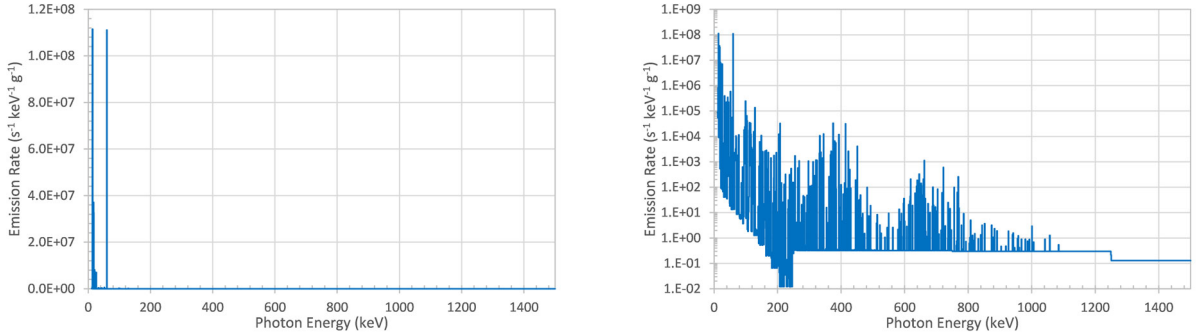

Figure 62. Emission spectrum for WGPu. (left) Linear vertical axis and (right) logarithmic vertical axis.

5.4 EQUIVALENT POINT SOURCE EMISSION SPECTRA

The SNM sources tend to emit many low-energy gamma rays that are easily attenuated by the SNM material itself and any metal containers. Because these sources do not scale simply with activity, different masses of these materials were simulated to include the self-attenuation and scattering within the material itself. The maximum sizes were chosen as 25 kg for the U materials and 8 kg for the Pu materials, which are the International Atomic Energy Agency (IAEA) [25] significant quantities: “the approximate amount of nuclear material for which the possibility of manufacturing a nuclear explosive device cannot be excluded.” The IAEA significant quantities are 8 kg for Pu, 25 kg for U that is 20% enriched in ^{235}U, and

75 kg for U with less than 20% ^{235}U. Significant quantities for natural U and DU are 10 and 20 tons, respectively.

For each of the U-based materials, five masses were simulated: 1, 2.5, 5, 10, and 25 kg. The radii were of these spheres were 2.324802, 3.155241, 3.975355, 5.008634, and 6.797762 cm, respectively. Similarly, for each of the Pu-based materials, the five masses simulated were 0.5, 1, 2, 4, and 8 kg, and the corresponding radii were 1.813916, 2.285391, 2.879412, 3.627832, and 4.570781 cm, respectively. These masses were simulated as spheres either bare or inside a spherical shell of steel 1 cm thick. The equivalent point source emission spectra are shown in Figures 63–67. Note that in these figures, except at very low energies, the curves seem to scale by surface area, indicating that the innermost portion of each sphere is well-shielded by the outer material.

The bare DU equivalent point source emission spectra distributions have uncertainties of approximately 0.5% at 100 keV, decreasing to 0.15% at 500 keV, and increasing to 0.2% at 1,000 keV, 0.4% at 1,500 keV, 1% at 1,800 keV, and 2.4% at 2,000 keV. When covered with 1 cm of steel, the uncertainties at 100 keV are 0.25%, dropping to 0.1% at 500 keV and increasing to 0.14% at 1,000 keV, 0.4% at 1,400 keV, 1% at 1,800 keV, and 2.8% at 2,000 keV.

The U ore, with all the daughters built up to equilibrium, has many more lines past 2,000 keV compared with the other U materials. For the bare ore, the uncertainties in the distributions are 1%–2% between 100 and 200 keV and fall from 0.6% at 200 keV to 0.2% at 400 keV, where they remain through 1,100 keV. Uncertainties rise to 0.3% at 1,760 keV. Between 1,760 keV and 2,200 keV, uncertainties range from 0.5% to 0.8%. From 2,200 to 2,450 keV, uncertainties are 1.3%–1.5% and from 2,450 to 2,700 keV are 5%. Above 2,700 keV, the uncertainties rise quickly as the distribution values fall. For the ore covered with 1 cm of steel, the uncertainties are similar to the bare ore except that in the range of 100–400 keV, uncertainties are 0.2%

The uncertainties of the bare refined U and LEU look very similar to the DU. This is also true for the uncertainties for the versions of U and LEU with 1 cm steel shielding—they are similar to the DU.

The uncertainties of the bare HEU are 1% from 100 to 1,000 keV, above which they increase to 3% at 1,500 keV, 5% at 1,700 keV, 10% at 1,900 keV, and 15%–20% from 1,900 to 2,000 keV. With 1 cm of steel, the uncertainties from 100 to 186 keV are 0.1%, rise steadily from 0.3% at 186 keV to 0.4% at 300 keV, and then increase to 0.8% at 1,000 keV. Above 1,000 keV, the uncertainties are similar or lower than the bare HEU.

The ^{238}Pu equivalent point source emission spectra distribution uncertainties from 100 to 150 keV are 5%–15%, 25–50% from 150 to 200 keV, and then dropping from 15% to 25% at 200 keV to 8%–14% at 300 keV. From 300 to 400 keV, uncertainties are 4.5%–7% and from 400 to 600 keV are 2%–4%. From 600–765 keV, uncertainties are 1.6%–2.7%. Above 765 keV, uncertainties increase to 4%–6% at 1,250 keV. Above 1,250 keV, uncertainties are 6%–9%. With 1 cm of steel, uncertainties are much lower: ≤0.2% for 100–765 keV and then rising from 0.2% at 765 keV to 0.7% at 1,500 keV.

PGPu without shielding has up to 20% uncertainties between 100 and 200 keV. At 200 keV, the 8% uncertainty falls to 5% at 300 keV. From 300 to 720 keV, uncertainties are 2%–4%. Above 720 keV, uncertainties climb to 8%–12% at 800 keV and remain steady to 1,250 keV. Above 1,250 keV, uncertainties are 12%–16%. For the shielded version of PGPu, uncertainties are lower with ≤0.3% from 100 to 660 keV, 0.5% for 660–720 keV, 1%–1.5% for 720–765 keV, and 2%–3% for 765–1,500 keV.

Bare FGPu has 8%–20% uncertainties between 100 and 200 keV. At 200 keV, the 4% uncertainty falls to 2.5% at 300 keV. From 300 to 720 keV, uncertainties are 1.5%–3.5%. Uncertainties are 5%–9% from 720

to 800 keV. From 800 to 1,250 keV, uncertainties are 5%–6.5% and above 1,250 keV are 6.5%–9%. With the steel shielding, uncertainties are 0.1%–0.2% from 100 to 412 keV, 0.25%–0.4% for 412–660 keV, 0.5%–1.3% for 660–765 keV, 1.2%–1.4% for 765–1,250 keV, and 1.7%–2% above 1,250 keV.

WGPu with no shielding has 5%–15% uncertainties between 100 and 200 keV. Between 200 and 300 keV, uncertainties are 1.4%–2%. From 300 to 720 keV, uncertainties are 1%–3%. From 720 to 1,000 keV, uncertainties are 3%–5.5% and from 1,000–1,250 keV are 4%–4.5%. Above 1,250 keV, uncertainties are 5%–7%. For the 1 cm of steel covering, uncertainties are 0.1%–0.25% from 100 to 412 keV, 0.25%–0.35% for 412–660 keV, 0.5%–0.7% for 660–765 keV, and 0.7%–1.2% for 765–1,000 keV. From 1,000 to 1,250 keV, uncertainties are 1%–1.3% and above 1,250 keV are 1.5%–1.8%.

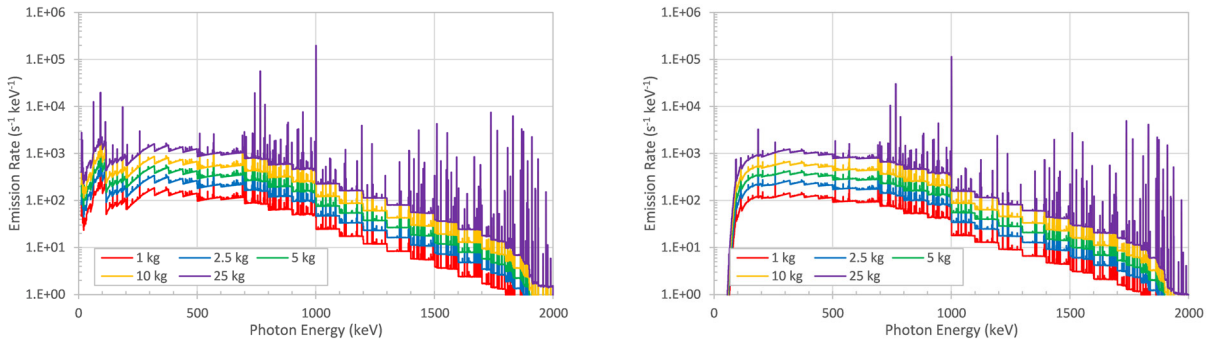

Figure 63. Equivalent point source emission spectra for DU. Left are bare spheres, and right are with 1 cm of steel.

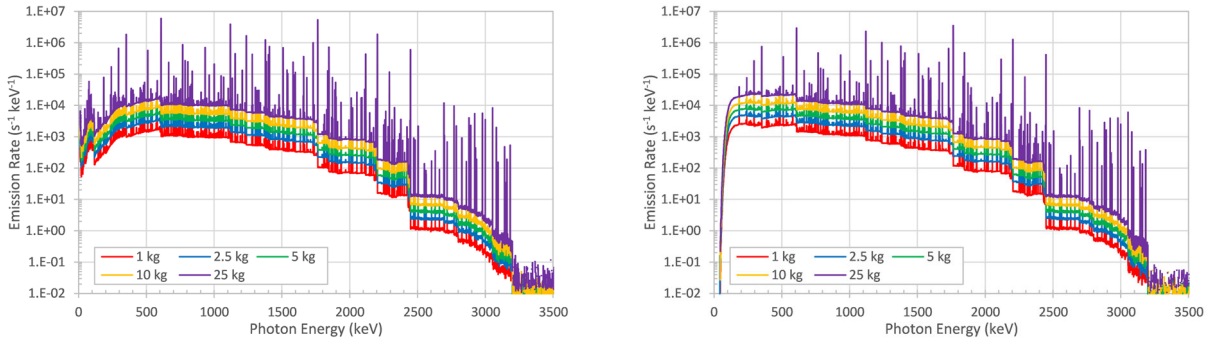

Figure 64. Equivalent point source emission spectra for U ore. Left are bare spheres, and right are with 1 cm of steel.

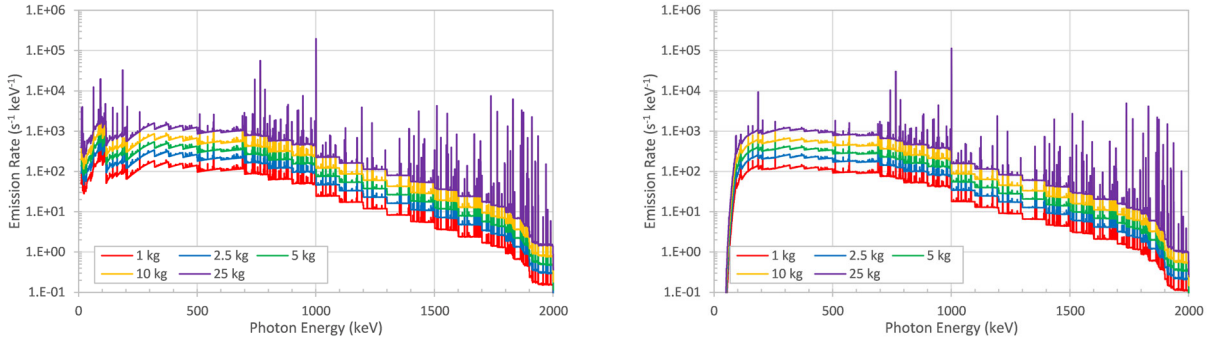

Figure 65. Equivalent point source emission spectra for refined U. Left are bare spheres, and right are with 1 cm of steel.

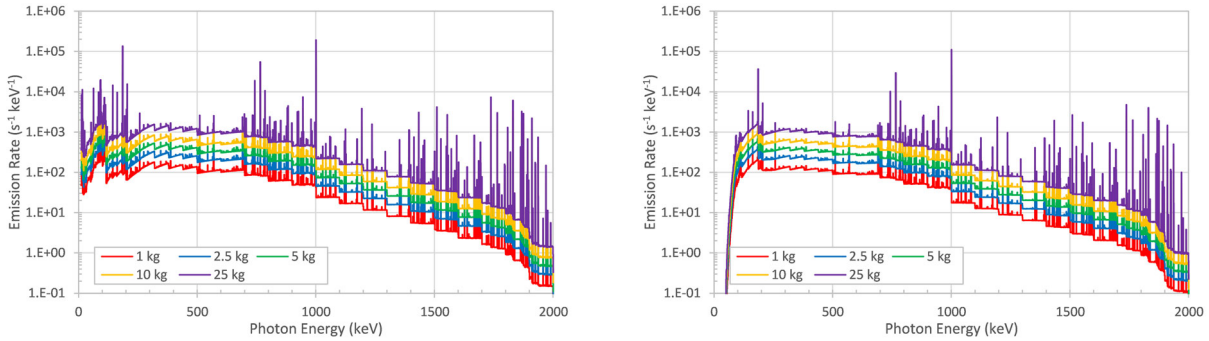

Figure 66. Equivalent point source emission spectra for LEU. Left are bare spheres, and right are with 1 cm of steel.

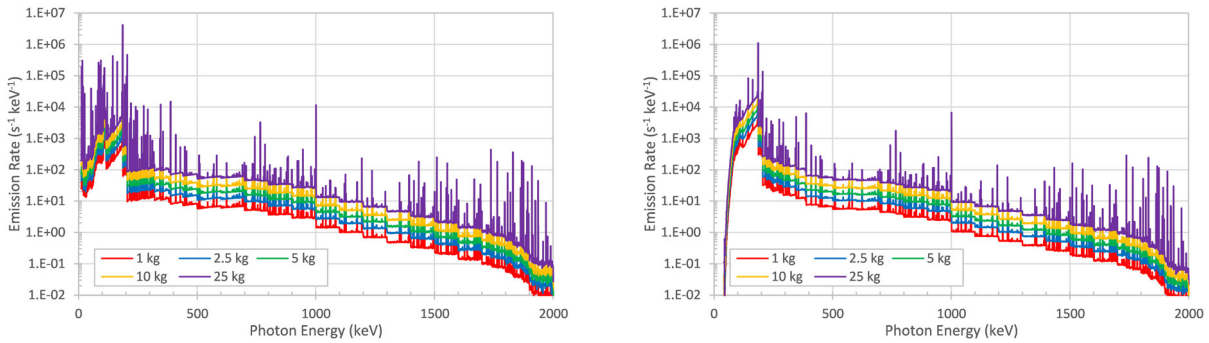

Figure 67. Equivalent point source emission spectra for HEU. Left are bare spheres, and right are with 1 cm of steel.

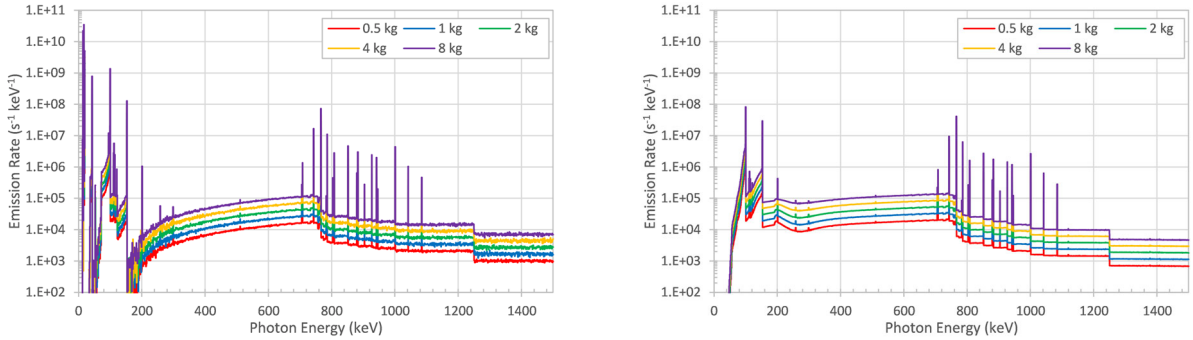

Figure 68. Equivalent point source emission spectra for ^{238}Pu. Left are bare spheres, and right are with 1 cm of steel.

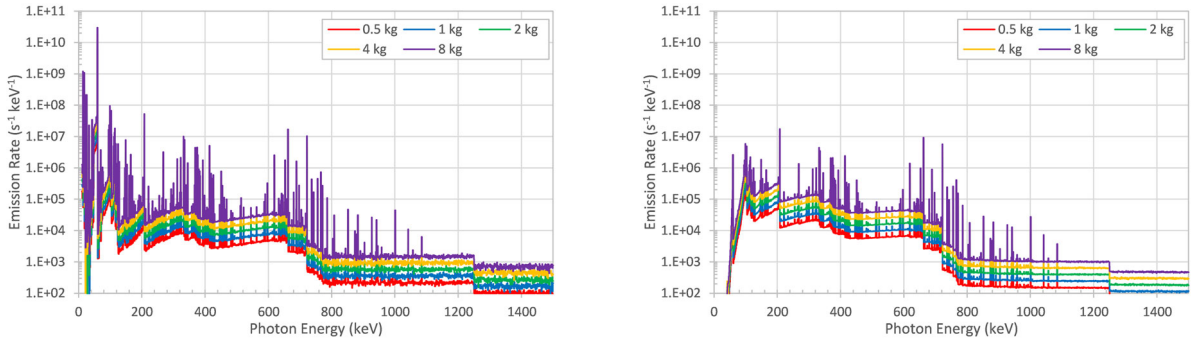

Figure 69. Equivalent point source emission spectra for PGPu. Left are bare spheres, and right are with 1 cm of steel.

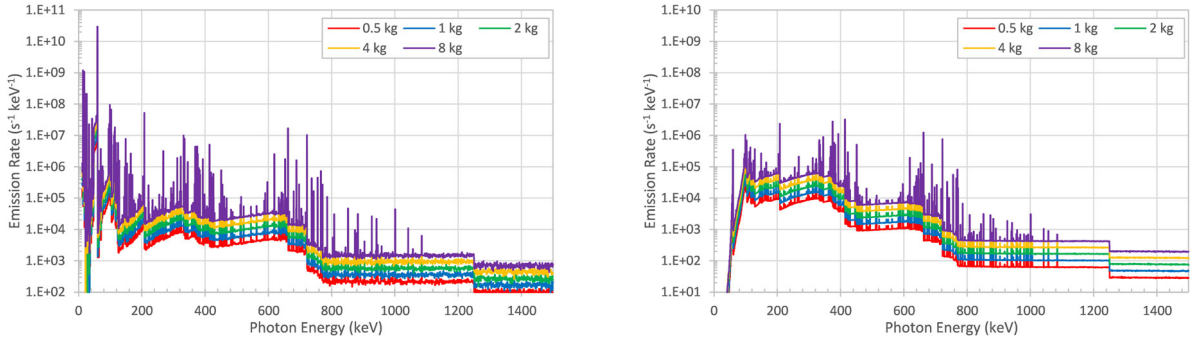

Figure 70. Equivalent point source emission spectra for FGPu. Left are bare spheres, and right are with 1 cm of steel.

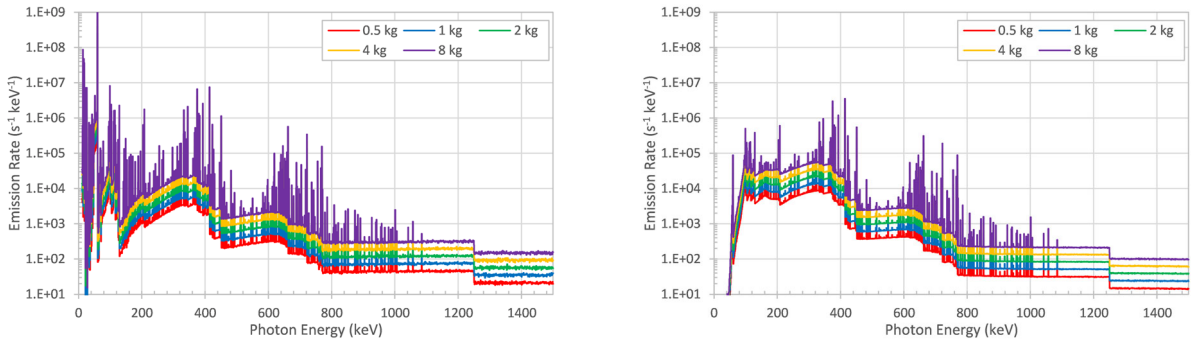

Figure 71. Equivalent point source emission spectra for WGPu. Left are bare spheres, and right are with 1 cm of steel.

Table 12 shows the emission strengths and equivalent point source strengths of the U and Pu sources. The maximum uncertainty for bare U equivalent point source strengths was 0.033%, for shieled U was 0.012%, for bare Pu was 0.164%, and for shielded Pu was 0.053%.

Table 12. Emission strengths and equivalent point source strengths of the U and Pu sources

Material	(kg)	Emission strength ORIGEN (s^{-1})	Equivalent point source strength (s^{-1}) bare	iron
DU	1	1.2194×10^{7}	1.6349×10^{5}	1.1760×10^{5}
	2.5	3.0484×10^{7}	3.0514×10^{5}	2.1930×10^{5}
	5	6.0969×10^{7}	4.8963×10^{5}	3.4977×10^{5}
	10	1.2194×10^{8}	7.8014×10^{5}	5.5175×10^{5}
	25	3.0484×10^{8}	1.4459×10^{6}	9.8975×10^{5}
U ore	1	6.1433×10^{7}	5.2970×10^{6}	4.5865×10^{6}
	2.5	1.5358×10^{8}	1.0137×10^{7}	8.7588×10^{6}
	5	3.0716×10^{8}	1.6433×10^{7}	1.4135×10^{7}
	10	6.1433×10^{8}	2.6418×10^{7}	2.2534×10^{7}
	25	1.5358×10^{9}	4.9242×10^{7}	4.0971×10^{7}
Ref. U	1	1.4387×10^{7}	1.6781×10^{5}	1.1884×10^{5}
	2.5	3.5967×10^{7}	3.1297×10^{5}	2.2151×10^{5}
	5	7.1934×10^{7}	5.0223×10^{5}	3.5322×10^{5}
	10	1.4387×10^{8}	7.9995×10^{5}	5.5698×10^{5}
	25	3.5967×10^{8}	1.4822×10^{6}	9.9858×10^{5}
LEU	1	2.3459×10^{7}	1.8679×10^{5}	1.2438×10^{5}
	2.5	5.8647×10^{7}	3.4769×10^{5}	2.3134×10^{5}
	5	1.1729×10^{8}	5.5733×10^{5}	3.6863×10^{5}
	10	2.3459×10^{8}	8.8734×10^{5}	5.8039×10^{5}
	25	5.8647×10^{8}	1.6429×10^{6}	1.0376×10^{6}
HEU	1	3.8193×10^{8}	9.3623×10^{5}	3.4286×10^{5}
	2.5	9.5482×10^{8}	1.7134×10^{6}	6.2031×10^{5}
	5	1.9096×10^{9}	2.7351×10^{6}	9.7523×10^{5}
	10	3.8193×10^{9}	4.3282×10^{6}	1.5021×10^{6}
	25	9.5482×10^{9}	7.9900×10^{6}	2.5750×10^{6}

Material	(kg)	Emission strength ORIGEN (s^{-1})	Equivalent point source strength (s^{-1}) bare	iron
^{238}Pu	0.5	3.0544×10^{13}	1.0260×10^{10}	5.0980×10^{7}
	1	6.1087×10^{13}	1.6383×10^{10}	8.1190×10^{7}
	2	1.2217×10^{14}	2.5845×10^{10}	1.2807×10^{8}
	4	2.4435×10^{14}	4.1084×10^{10}	2.0058×10^{8}
	8	4.8870×10^{14}	6.4461×10^{10}	3.0777×10^{8}
RGPu	0.5	3.3486×10^{12}	5.3950×10^{9}	2.5389×10^{7}
	1	6.6972×10^{12}	8.6011×10^{9}	4.0256×10^{7}
	2	1.3394×10^{13}	1.3597×10^{10}	6.3370×10^{7}
	4	2.6789×10^{13}	2.1629×10^{10}	9.9369×10^{7}
	8	5.3578×10^{13}	3.3818×10^{10}	1.5279×10^{8}
FGPu	0.5	4.9980×10^{11}	7.4807×10^{8}	6.9274×10^{6}
	1	9.9961×10^{11}	1.1929×10^{9}	1.0998×10^{7}
	2	1.9992×10^{12}	1.8853×10^{9}	1.7355×10^{7}
	4	3.9984×10^{12}	2.9968×10^{9}	2.7283×10^{7}
	8	7.9969×10^{12}	4.6900×10^{9}	4.2223×10^{7}
WGPu	0.5	1.6311×10^{11}	2.0469×10^{8}	4.9525×10^{6}
	1	3.2623×10^{11}	3.2631×10^{8}	7.8615×10^{6}
	2	6.5246×10^{11}	5.1580×10^{8}	1.2425×10^{7}
	4	1.3049×10^{12}	8.1947×10^{8}	1.9575×10^{7}
	8	2.6098×10^{12}	1.2822×10^{9}	3.0424×10^{7}

5.5 ESTIMATED SODIUM IODIDE DETECTOR RESPONSES

The simulated responses of a NaI detector (2 × 4 × 16 in., with photons striking the largest face) to these SNM sources are shown in Figures 68–76. In each figure, five curves are shown for the five different masses. In all materials, the smallest sizes produce the lowest count rates.

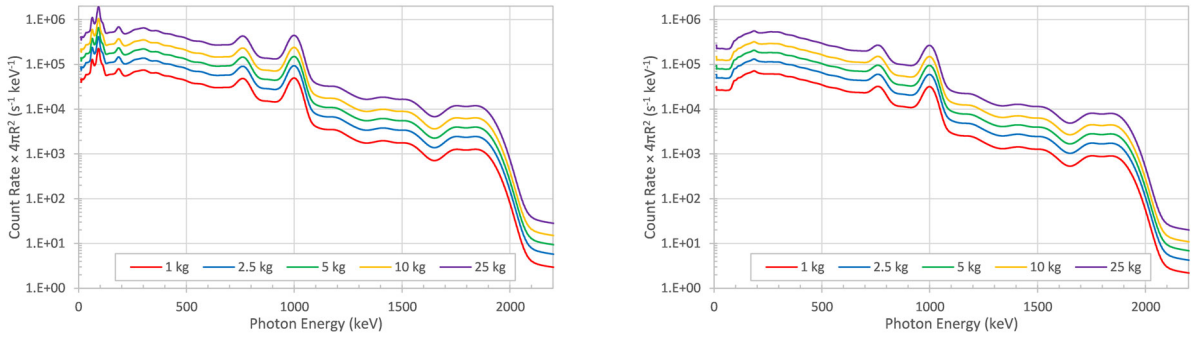

Figure 72. Predicted NaI count rate spectra for DU. Left are bare spheres, and right are with 1 cm of steel.

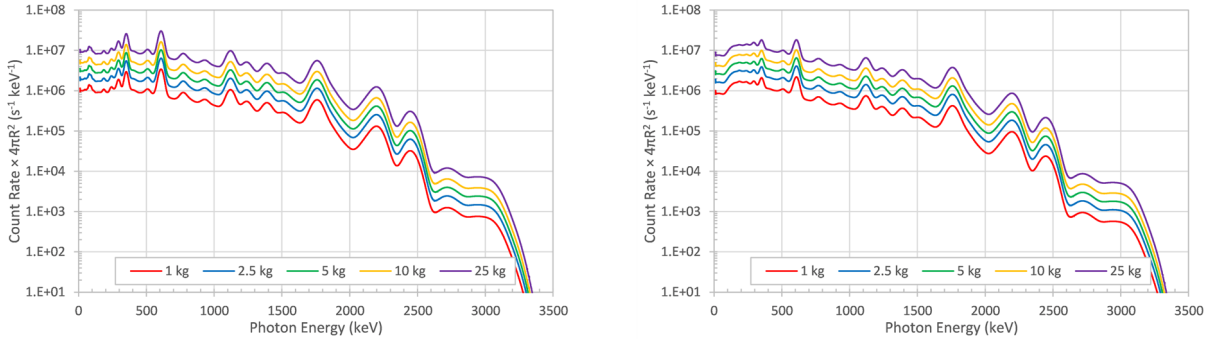

Figure 73. Predicted NaI count rate spectra for U ore. Left are bare spheres, and right are with 1 cm of steel.

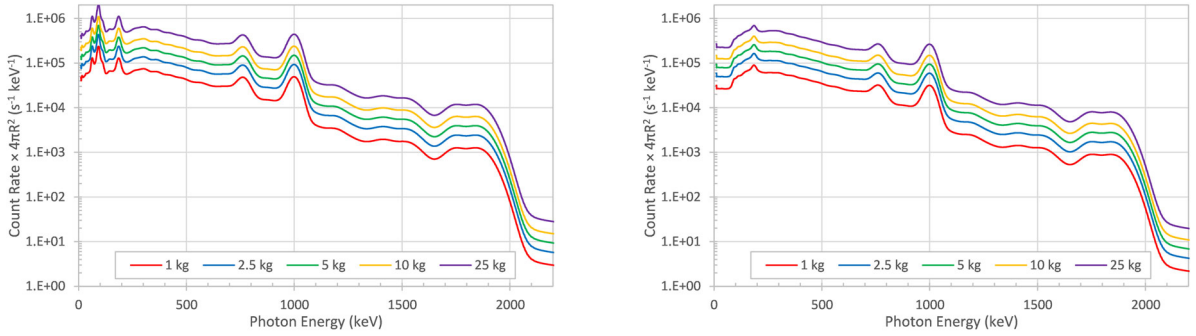

Figure 74. Predicted NaI count rate spectra for refined U. Left are bare spheres, and right are with 1 cm of steel.

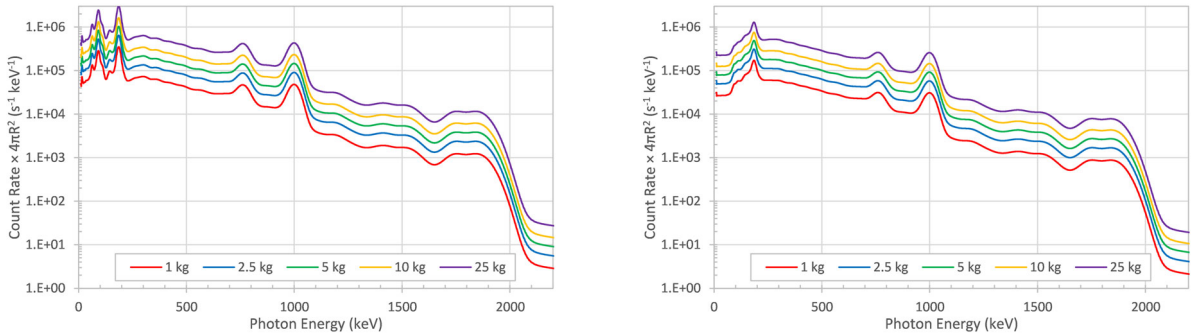

Figure 75. Predicted NaI count rate spectra for LEU. Left are bare spheres, and right are with 1 cm of steel.

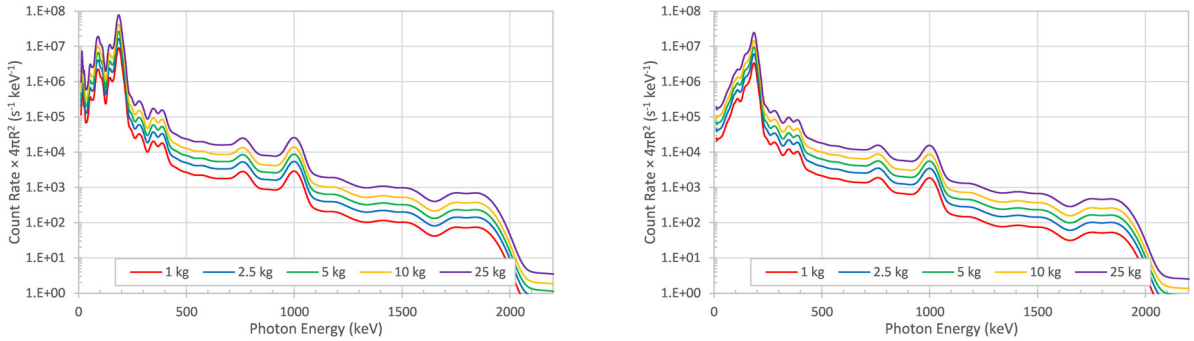

Figure 76. Predicted NaI count rate spectra for HEU. Left are bare spheres, and right are with 1 cm of steel.

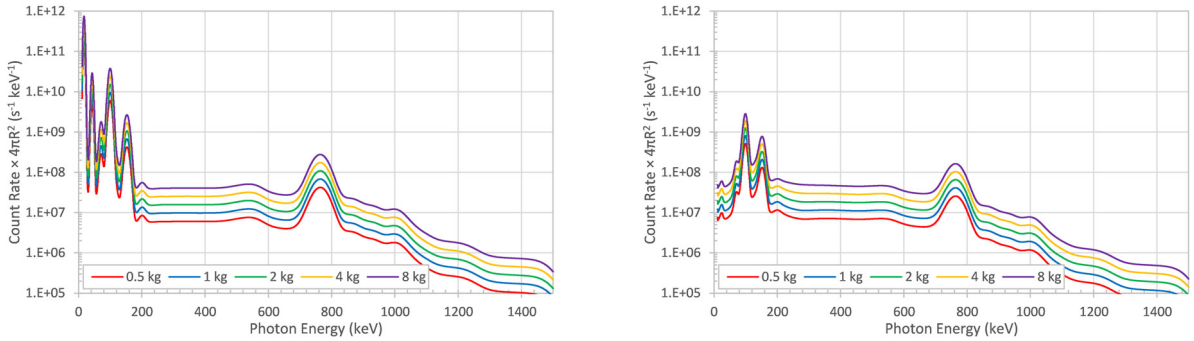

Figure 77. Predicted NaI count rate spectra for ^{238}Pu. Left are bare spheres, and right are with 1 cm of steel.

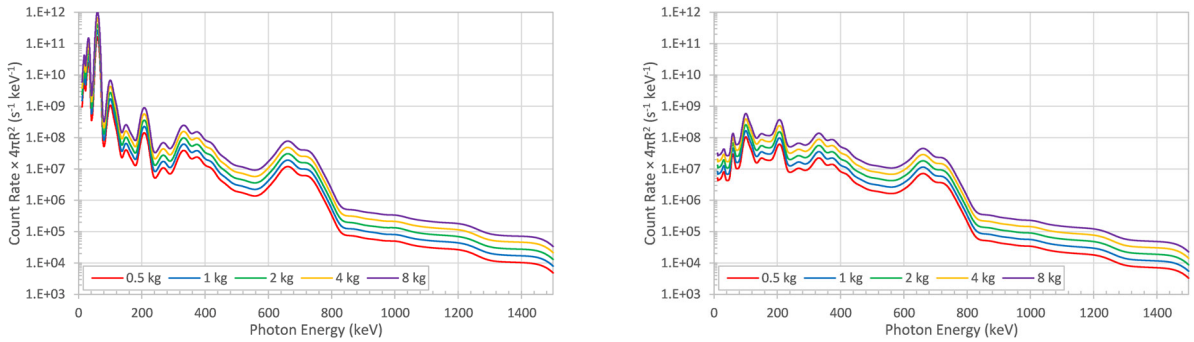

Figure 78. Predicted NaI count rate spectra for PGPu. Left are bare spheres, and right are with 1 cm of steel.

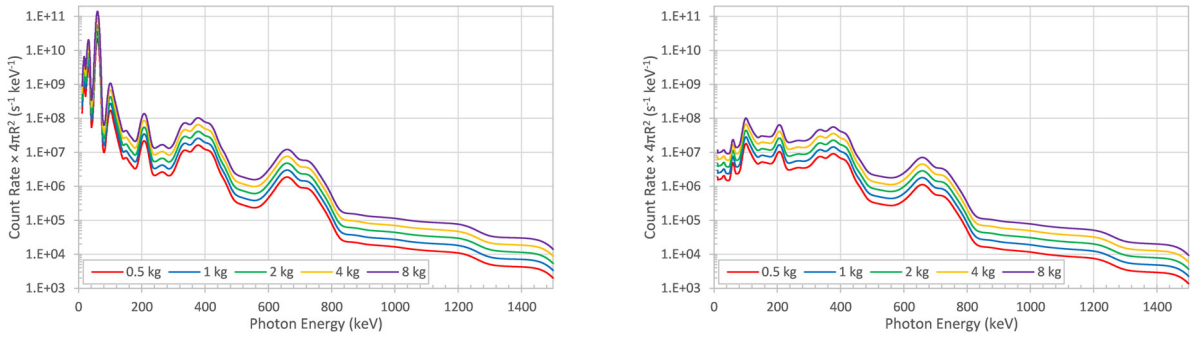

Figure 79. Predicted NaI count rate spectra for FGPu. Left are bare spheres, and right are with 1 cm of steel.

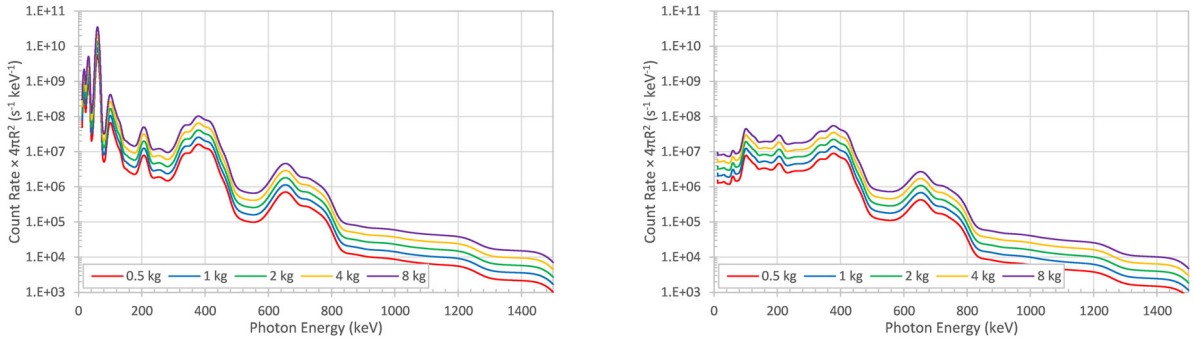

Figure 80. Predicted NaI count rate spectra for WGPu. Left are bare spheres, and right are with 1 cm of steel.

6. SUMMARY

In total, 142 threat sources were developed for the RADAI and REX projects and can be used for other detection/modeling projects. The equivalent point source distributions can be used in a larger geometry as a point model of a small source that already includes the effect of any self-shielding and any additional shielding material. The equivalent point source magnitudes represent how many photons per second would escape from the outer layer of each source.

The final threat source emission spectra for the basic isotopes, medical isotopes, industrial isotopes, and SNMs have been formatted for three transport codes: MCNP, SCALE/MAVRIC, and Omnibus/Shift [26]. The MCNP files use the *.i extension, the MAVRIC files use the *.dist.txt extension, and the Shift files use the *.omn extension. These files are listed in Table 13 and are available within the RADAI project on the bdc.lbl.gov data portal (account required) or may be requested via email directly from the authors. The data for each file type are displayed in a binned histogram, and each file contains a comment with the total photon emission rate in units of inverse second-becquerels or inverse seconds (for the SNM materials) as a reminder to the user to include that factor in any tally multipliers. The files are all ASCII text, so any of the three formats can be easily reformatted for other codes.

Table 13. Equivalent point source emission spectra files for MCNP, SCALE/MAVRIC, and Shift

Source		Base file name (*.i, *.dist.txt, or *.omn)		
Basic Isotopes	^{40}K	19_K_040bare	19_K_040steel	19_K_040pmma
	^{57}Co	27_Co057bare	27_Co057steel	27_Co057pmma
	^{60}Co	27_Co060bare	27_Co060steel	27_Co060pmma
	^{137}Cs	55_Cs137bare	55_Cs137steel	55_Cs137pmma
	^{133}Ba	56_Ba133bare	56_Ba133steel	56_Ba133pmma
	^{192}Ir	77_Ir192bare	77_Ir192steel	77_Ir192pmma
	^{226}Ra	88_Ra226bare	88_Ra226steel	88_Ra226pmma
	^{232}Th	90_Th232bare	90_Th232steel	90_Th232pmma
	^{241}Am	95_Am241bare	95_Am241steel	95_Am241pmma
Medical	^{18}F	09_F_018	^{133}Xe	54_Xe133
	^{67}Ga	31_Ga067	^{177}Lu	71_Lu177
	^{99m}Tc	43_Tc99m	^{201}Tl	81_Tl201
	^{131}I	53_I_131		
Indust.	^{67}Cu	29_Cu067bare	29_Cu06steel	
	^{90}Sr	38_Sr090alum1	38_Sr090alum2	
	^{192}Ir	77_Ir192steel2	77_Ir192steel5	
^{192}Ir in DU Shell	^{192}Ir	77_Ir192uran05	Depleted U	DUshell05
	^{192}Ir	77_Ir192uran10	Depleted U	DUshell10
	^{192}Ir	77_Ir192uran15	Depleted U	DUshell15
	^{192}Ir	77_Ir192uran20	Depleted U	DUshell20
	^{192}Ir	77_Ir192uran25	Depleted U	DUshell25
	^{192}Ir	77_Ir192uran30	Depleted U	DUshell30
Special Nuclear Materials	Depl. U	1_DUbare*X*	1_DUiron*X*	
	U ore	2_NatUbare*X*	2_NatUiron*X*	
	Ref. U	3_RefUbare*X*	3_RefUiron*X*	
	LEU	4_LEUbare*X*	4_LEUiron*X*	
	HEU	5_HEUbare*X*	5_HEUiron*X*	
	^{238}Pu	6_Pu238bare*X*	6_Pu238iron*X*	
	PGPu	7_PGPubare*X*	7_PGPuiron*X*	
	FGPu	8_FGPubare*X*	8_FGPuiron*X*	
	WGPu	9_WGPubare*X*	9_WGPuiron*X*	

Basic: “bare” is 0.25 mm steel, “steel” is 1 cm of steel, “pmma” is 1.25 cm of PMMA.
Industrial: “bare” and “steel” are 0.25 mm and 1 cm of steel; Al and steel amounts in cm.
^{192}Ir and DU shells—use together, only scale ^{192}Ir, shell thicknesses in mm.
For SNM materials: “bare” is no shielding, “iron” is 1 cm of steel.
For U materials, *X* is 1–5 for masses of: 1, 2.5, 5, 10, and 25 kg.
For Pu materials, *X* is 1–5 for masses of: 0.5, 1, 2, 4, and 8 kg.

7. REFERENCES

[1] James M. Ghawaly Jr., Andrew D. Nicholson, Douglas E. Peplow, Christine M. Anderson-Cook, Kary L. Myers, Daniel E. Archer, Michael J. Willis, and Brian J. Quiter, "Data for Training and Testing Radiation Detection Algorithms in an Urban Environment," *Scientific Data* 7, no. 328 (2020). https://doi.org/10.1038/s41597-020-00672-2.

[2] Andrew D. Nicholson, Douglas E. Peplow, James M. Ghawaly, Michael J. Willis, and Daniel E. Archer, "Generation of Synthetic Data for a Radiation Detection Algorithm Competition," *IEEE Transactions on Nuclear Science* 67, no. 8 (2020): 1968–1975. https://doi.org/10.1109/TNS.2020.3001754.

[3] Andrew D. Nicholson, Douglas E. Peplow, Christine M. Anderson-Cook, Christopher R. Greulich, James M. Ghawaly Jr., Kary L. Myers, Daniel E. Archer, Michael J. Willis, and Brian J. Quiter, "Data for Training and Testing Radiation Detection Algorithms in an Urban Environment," Oak Ridge National Laboratory, February 2020. https://doi.ccs.ornl.gov/ui/doi/74.

[4] American National Standards Institute, *Performance Criteria for Handheld Instruments for the Detection and Identification of Radionuclides*, ANSI N42.34 (November 2015).

[5] American National Standards Institute, *Evaluation and Performance of Radiation Detection Portal Monitors for Use in Homeland Security*, ANSI N42.35 (March 2016).

[6] American National Standards Institute, *Performance Criteria for Spectroscopy-Based Portal Monitors Used in Homeland Security*, ANSI N42.38 (June 2015).

[7] American National Standards Institute, *Performance Criteria for Mobile and Transportable Radiation Monitors Used for Homeland Security*, ANSI N42.43 (April 2016).

[8] American National Standards Institute, *Performance Criteria for Backpack-Based Radiation-Detection Systems Used for Homeland Security*, ANSI N42.53 (June 2013).

[9] W. A. Wieselquist and R. A. Lefebvre, eds., *SCALE 6.3.0 User Manual*, ORNL/TM-SCALE-6.3.0 (Oak Ridge, Tennessee: Oak Ridge National Laboratory, December 2021).

[10] CBRNE Central Staff, "Wearable Intelligent Nuclear Detection (WIND)," CBRNE Central, accessed August 2023, https://cbrnecentral.com/wearable-intelligent-nuclear-detection-wind/3228/.

[11] Michael J. Willis, James M. Ghawaly Jr., Nicholas J. Prins, Brandon R. Longmire, Andrew J. Rowe, and Daniel E. Archer, *Wearable Intelligent Nuclear Detection (WIND) Characterization Report*, ORNL/TM-2022/2563 (Oak Ridge, Tennessee: Oak Ridge National Laboratory, September 2022).

[12] Ronald J. McConn Jr., Christopher J. Gesh, Richard T. Pagh, Robert A. Rucker, and Robert G. Williams III, *Compendium of Material Composition Data for Radiation Transport Modeling*, PIET-43741-TM-963, PNNL-15870, Rev. 1 (Richland, Washington: Pacific Northwest National Laboratory, March 2011). https://www.pnnl.gov/main/publications/external/technical_reports/PNNL-15870Rev1.pdf.

[13] World Health Organization, "Gallium Citrate Injection," *The International Pharmacopoeia—Ninth Edition*, published 2019, accessed December 6, 2020. https://apps.who.int/phint/en/p/docf/.

[14] "Gallium Citrate Ga 67," Drugs.com, accessed December 6, 2016, https://www.drugs.com/pro/gallium-citrate-ga-67.html.

[15] IAEA Human Health Campus, "Product Issues with Eluted ^{99m}Tc," International Atomic Energy Agency, accessed December 6, 2016, https://humanhealth.iaea.org/HHW/Radiopharmacy/VirRad/Eluting_the_Generator/Generator_Module/Elution_of_the_99Mo99mTc_generator/Product_issues_with_eluted_99mTc/index.html.

[16] Council of Europe, "Sodium Iodide (131I) Capsules for Diagnostic Use," *European Pharmacopoeia 5.0*, 01/2005:0938 (Strasbourg, France: 2005).

[17] S. Staelens, T. de Wit, I. Lemahieu, and F. Beekman, "Significant Septal Penetration Effects Caused by Impurities in Cyclotron-Produced Thallium-201," *The Journal of Nuclear Medicine* 47 (2006).

[18] F. Groppi, M. Bonardi, C. Birattari, L. Gini, M. Severgnini, and C. Mainardi, *A Rapid Improved Method for Gamma-Spectrometry Determination of Thallium-202 Impurities in [Thallium-201] Labelled Radiopharmaceuticals*, INFN/TC-01/18 (Rome, Italy: Istituto Nazionale Di Fisica Nucleare, November 28, 2001). https://doi.org/10.15161/oar.it/1448986128.37.

[19] Gregory G. Thoreson, *Detecting Radiation Algorithms Group (DRAG)*, SAND2021-3122PE-694854 (Albuquerque, New Mexico: Sandia National Laboratories, March 2021).

[20] "Xenon Xe 133 Gas Prescribing Information," Drugs.com, accessed June 2022, https://www.drugs.com/pro/xenon-xe-133-gas.html.

[21] R. A. Kuznetsov, et al., "Production of Lutetium-177: Process Aspects," *Radiochemistry* 61 (2019): 381–395. https://doi.org/10.1134/S1066362219040015.

[22] C. J. Werner, ed., *MCNP User's Manual—Code Version 6.2*, LA-UR-17-29981 (Los Alamos, New Mexico: Los Alamos Laboratory, October 2017). http://permalink.lanl.gov/object/tr?what=info:lanl-repo/lareport/LA-UR-17-29981.

[23] Michael W. Enghauser, *FRMAC Gamma Spectroscopist Knowledge Guide*, SAND2019-9768 R (Albuquerque, New Mexico: Sandia National Laboratories, August 2019). https://doi.org/10.2172/1763003.

[24] US Department of Energy, *Stabilization, Packaging and Storage of Plutonium-Bearing Materials*, DOE Standard 3013-2018 (Washington, DC: US Department of Energy, November 2018). https://rampac.energy.gov/docs/default-source/doe-requirements/doe-std-3013-2018.pdf.

[25] International Atomic Energy Agency, *IAEA Safeguards Glossary*, 2001 Edition, International Nuclear Verification Series No. 3, 2001 Edition (Vienna, Austria: International Atomic Energy Agency, 2002). https://www-pub.iaea.org/MTCD/Publications/PDF/nvs-3-cd/pdf/NVS3_prn.pdf.

[26] Steven P. Hamilton, Thomas M. Evans, Katherine E. Royston, and Elliott D. Biondo, "Domain Decomposition in the GPU-Accelerated Shift Monte Carlo Code," *Annals of Nuclear Energy* 166, no. 1 (2022). https://doi.org/10.1016/j.anucene.2021.108687.